Supplemental Text: An Optimal Regulation of Fluxes Dictates Microbial Growth In and Out of Steady-State

Griffin Chure and Jonas Cremer

Department of Biology, Stanford University, Stanford, CA, USA.

gchure@stanford.edu, jbcremer@stanford.edu

January 27, 2022

Contents

1 Allocation models to study microbial growth **2**

2 The maintenance of macromolecular densities promotes a simple model based on rates **3**
2.1 On neglecting spatiotemporal aspects of the cell . . . 3
2.2 Approximating concentration via relative abundance . . . 3

3 Estimating the number of ribosomes within the cell **3**

4 Ribosomes making ribosomes - a consideration of rRNA synthesis **4**

5 Precursors concentrations and the importance of dilution by cell growth **5**

6 Derivation of Analytical Expressions **6**
6.1 Deriving the Steady-State Growth Rate . . . 6
6.2 Defining ϕ_{Rb} For Scenarios II and III . . . 7
6.2.1 Scenario II: Constant Translation Rate . . . 7
6.2.2 Scenario III: Optimal Allocation . . . 8

7 Additional considerations relevant at slow growth **8**
7.1 Active protein degradation . . . 8
7.2 Observations not in steady-state . . . 9
7.3 Inactive ribosomes . . . 9

8 What makes the fraction of "other" proteins? **11**
8.1 Defining the other proteins . . . 11
8.2 Neglecting the other proteins . . . 12

9 Inactive ribosomes are not needed to describe the linear relation between ribosome content and growth rate **13**

10 Application of the Model to *Saccharomyces cerevisiae* **14**

11 Implementing Flux-Parity Regulation via ppGpp **14**
11.1 Formulation of model . . . 15
11.2 Optimal allocation emerges from flux-parity regulation . . . 17
11.3 Parameter dependence of the flux-parity model . . . 17
11.4 Incorporating effects of ribosome-targeting antibiotics . . . 19
11.5 Incorporating effects of excess protein stress . . . 20
11.6 Incorporating effects of nutrient upshifts . . . 21
11.7 Incorporating effects of nutrient depletion . . . 21

12 Data Sets **21**

13 Supplementary Tables **21**

1 Allocation models to study microbial growth

Over the past several decades, theoretical studies have introduced a huge variety of mathematical models to better understand how microbes grow. These range from the relatively simple phenomenological relations introduced by Verhulst [1] and Monod [2] to describe exponential growth and nutrient consumption to high-dimensional models [3–5] which explicitly model hundreds of cellular processes involved in biomass synthesis. Here, we specifically summarize other low-dimensional modeling approaches which integrate considerations of protein synthesis and metabolism.

As is outlined in the introduction of the main text, the idea that protein synthesis constitutes a major limitation of microbial growth has a storied history. With an ever-improving characterization of both the cellular composition and the major biochemical processes undertaken by microbes, it has become increasingly clear that the auto-catalytic nature of protein synthesis (i.e. "ribosomes making ribosomes") and the corresponding allocation of ribosomal activity towards different proteins are of paramount importance. Therefore, it is imperative to consider them when aiming for a more mechanistic understanding of growth [6–8] and several low-dimensional allocation models have been introduced.

In a seminal work, Molenaar *et al.* [9] introduced for example a low-dimensional model of protein synthesis to investigate the growth-rate dependent switch between different metabolic pathways. Central to this model is a consideration of how resources are partitioned among four different protein classes, including ribosomal and metabolic proteins. Through enumerating coupled differential equations that relate the allocation to growth rate, their model predicts that ribosome content needs to scale linearly with growth-rate to ensure rapid growth. A similar low-dimensional allocation framework based on similar differential equations was introduced by Scott *et al.* [10]. This work extended the authors' previous experimental study [11] which introduced phenomenological relations describing ribosome content and its dependence on the growth conditions. The authors discuss how their dynamical allocation model could lead to the observed scaling, but the biological meaning behind some model parameters is largely conjecture as the study does not include a more direct comparison between the prediction of the allocation model and experimental data. In the years that followed, several studies reformulated these models to consider more explicitly how the global regulator guanosine tetraphosphate (ppGpp) may tune the allocation of ribosomes to obtain optimal growth across conditions, specifically in *Escherichia coli* [12–14]. These models take a very fine-grained view of the kinetics of ppGpp synthesis, its degradation, and its dependence on stalled ribosomes. In some cases, particular details of the kinetics of transcriptional initiation of ribosomal RNA genes is explicitly considered [13]. A commonality between these models is again an enumeration of a handful of coupled ordinary differential equations, though their precise forms are unique. These theoretical analyses suggested that the ppGpp mediated regulation feedback can robustly tune ribosome content with encountered conditions to support optimal growth. However, the evaluation of these models (namely, Bosdriesz *et al.* and Giordano *et al.* [12, 13]) is significantly hampered due to a cursory and largely qualitative comparison with data, considering only the scaling of ribosome content with growth rate (Bosdriesz *et al.* [13] and Giordano *et al.* [12]) or the influence of translation-limiting antibiotics (Giordano *et al.*). Furthermore, Wu *et al.* [14] recently made a suite of measurements of relative ppGpp concentrations under various conditions and presented an model to understand their observations. In contrast to our approach, they focus on the role of inactive ribosomes (which we neglect in Sec. 7.3). They contend that a condition-dependent translation rate is at odds with the principle of optimal allocation and cannot be understood without explicit consideration of an inactive ribosome pool. We believe that our work, however, illustrates that a condition-dependent translation rate *supports* a picture of optimal allocation without requiring an inactive pool.

Our approach is similar in spirit to these models as a collective with an allocation of resources as a central component. However, our study goes significantly beyond published studies in several respects. In particular, our approach emphasizes the dynamics rather than exclusively focusing on the steady-state regime. Furthermore, rather than using observed steady-state relations to inform the construction of the model, we instead build a general dynamical model and use the steady-state regime as a means to test the model's validity. To our knowledge, there are no studies which formulated allocation models covering out of steady-state dynamics from first principles without the involvement of phenomenological parameters. Furthermore, we derive in this work several novel analytical and numerical solutions to describe growth in a broad range of growth conditions and for different allocation strategies. Building on this analysis we perform an extensive one-to-one comparison with very different experimental observations. The comparison, which is based on a combined data set covering ≈ 50 studies, confirms that the theory can describe observations in quantitative accuracy without the adjustment of major model parameters from one scenario to the next.

2 The maintenance of macromolecular densities promotes a simple model based on rates

2.1 On neglecting spatiotemporal aspects of the cell

The low-dimensional theory we derive in this work is completely ignorant to (i) the spatial arrangement of processes across the cell and (ii) neglects the existence of cells as a whole. Instead, we chose a description which only considers the change of total protein biomass of the system (i.e. culture) over time. Despite this objectively major simplification, the model quantitatively predicts growth phenotypes across a broad range of conditions, as we presented in the main text. Remarkably, this is accomplished with one core set of parameters which remains fixed across conditions. To us, this is a surprising result given that cell size and the spatio-temporal arrangement of cellular components are known to be highly dependent on conditions, which in principle should affect major model parameters, such as the maximal speed of translation. The finding that the model can nevertheless capture observations across conditions suggest that many cellular processes, including those involved in cell size control, are highly coordinated by the cell such that translation and metabolism work efficiently and can be captured by simple rate equations; it is the complexity of the cellular machinery which allows us to formulate a simple but predictive model of growth.

To illustrate this point, we can consider the density of macromolecules within the cell which strongly informs the rates of myriad biochemical reactions. A density that is too large, for example, will strongly hamper diffusion and thus slow many reaction rates, while a low density generally reduces binding rates [15, 16]. Cells are thus expected to maintain macro-molecular density ranges within narrow ranges to operate efficiently [15]. Experimental studies support this idea. For example, mass densities in *E. coli* appear to be restricted within narrow ranges across growth conditions [17]. Complex biophysical processes appear to also be in place to control the spatial arrangement of macromolecules, such as the strong mutual-exclusivity of DNA and ribosomes within the cytoplasm [18]. If it were not for these processes, macromolecular densities and thus major cellular processes (like translation) would vary tremendously with growth conditions and a model based on simple rate equations would have very limited predictive power.

2.2 Approximating concentration via relative abundance

In addition to maintaining the *total* macromolecular densities, cells also maintain an approximately constant protein density [19]. This observation allows us to make a major simplification in formulating our allocation model, namely the approximation of concentrations as relative mass abundances. The rate γ at which ribosomes can synthesize protein is dependent on the abundance of precursors, c_{pc}, in the cell. To compute the concentration and/or density in typical units (e.g. μM, or mass / volume), we would require some measure of the total cellular volume, V_{cell}, such that the concentration follows

$$c_{pc} = \frac{M_{pc}}{V_{cell}}, \tag{S1}$$

with M_{pc} denoting the total mass of the precursor pool. By making the experimentally-supported assertion that the protein density ρ is constant, we can say that

$$\rho = \frac{M}{V_{cell}} = \text{Constant}, \tag{S2}$$

where M is the total protein biomass. Thus, the total cellular volume V_{cell} can be computed as

$$V_{cell} = \frac{M}{\rho}. \tag{S3}$$

Plugging this result into Eq. S1, we arrive at the approximation

$$c_{pc} = \rho \frac{M_{pc}}{M} \approx \frac{M_{pc}}{M}. \tag{S4}$$

In this work, we neglect ρ as a multiplicative constant, and treat c_{pc} as being dimensionless. We direct the reader to Refs. [11] and [20] for a further discussion of the conversion between concentration and relative abundance.

3 Estimating the number of ribosomes within the cell

In the main text, we make the assertion that the accumulation of biomass is dependent on two factors: (i) the number of ribosomes present in the cell and (ii) the speed at which they make peptide bonds. Here we clarify how we estimate the number of ribosomes in the cell.

Ribosomal assembly is an impressively complex process in which $\approx$ 50 individual proteins and three large rRNAs self-assemble into two major subunits with high efficiency [21]. In this work, we thus assume that assembly is instantaneous with the total number of ribosomes given by the total mass of ribosomal proteins, M_{Rb}/m_{Rb}, where m_{Rb} is the proteinaceous mass of a single ribosome. In reality, ribosomes can only begin translation once they are assembled. Therefore, a proper accounting of the mass of *functional* ribosomes is

$$N_{Rb} = \left\lfloor \frac{M_{Rb}}{m_{Rb}} \right\rfloor \leq \frac{M_{Rb}}{m_{Rb}}, \tag{S5}$$

where the brackets $\lfloor \dots \rfloor$ denote the floor function (i.e., rounding down to the nearest integer). Given number of ribosomes per cell is typically large (between ≈ 5000 and $\approx 20{,}000$ depending on the condition [22]), the fraction of incomplete ribosomal mass is comparatively small, allowing us to make the approximation

$$\left\lfloor \frac{M_{Rb}}{m_{Rb}} \right\rfloor \approx \frac{M_{Rb}}{m_{Rb}}. \tag{S6}$$

If cells could consist exclusively of ribosomes (meaning, $M_{Rb} = M$) which are translating at their maximal rate, $\gamma_{max} = v_{tl,max}/m_{Rb}$, the total biomass dynamics would become

$$\frac{dM}{dt} = \frac{dM_{Rb}}{dt} = \gamma_{max} M_{Rb}, \tag{S7}$$

which can be solved as an exponential relation with a doubling time of

$$t_{double} = \log 2 \frac{1}{\gamma_{max}} = \log 2 \frac{m_{Rb}}{v_{tl,max}}. \tag{S8}$$

Notably, this approximation only holds as ribosomes consist of many short ribosomal proteins (each $\approx$ 200-500 amino acids in size) which are quickly translated. With many different ribosomes translating, all ribosomal proteins required to form a novel ribosome can be translated very quickly [21]. Conversely, if the proteinaceous components of ribosomes was a *single* protein with ≈ 7500 amino acids, then the shortest doubling time would instead be the time it takes to translate a protein with mass m_{Rb} (i.e., $t_{double} = m_{Rb}/v_{tl,max}$), and a description with a simple rate equation (Eq. S5) would substantially overestimate protein synthesis. This is again emphasizing that complex cellular processes need to be in place for a simple rate equation formulation to work.

4 Ribosomes making ribosomes - a consideration of rRNA synthesis

The allocation model presented in the main text considers exclusively protein synthesis as the determinant of microbial growth. Yet, as the cell contains a substantial mass of RNA, microbes clearly must allocate some fraction of their ribosomes towards the synthesis of RNA polymerases (RNAP) such that the required RNA species (rRNA, mRNA, and tRNA) can accumulate to the appropriate levels. To what extent does this process affect growth? Recent order-of-magnitude work has shown that the abundance of RNAP (and the corresponding σ-factors) is not limiting for growth of *Escherichia coli* [22]. Here we additionally show that RNA synthesis is not associated with a huge protein cost and RNAP synthesis (and correspondingly, RNA synthesis) has thus only a minor effect on the growth rate in nutrient replete conditions (the situation can be different in nutrient deplete conditions, for example when phosphate to support RNA synthesis is limiting growth).

Ribosomal RNA (rRNA) accounts for the vast majority of RNA in the cell ($\approx$ 85%; BNID: 106421 [23]) and we therefore only consider the synthesis of rRNA to estimate the demand for RNAP. Ribosomes consist of three large rRNA species which together account for a large fraction of the ribosomal mass and are responsible for the catalysis of peptide bonds. It thus follows that rRNA accounts for a large fraction of the cellular dry mass. One may therefore expect rRNA synthesis to be an important determinant of the time it takes to replicate a ribosome with a strong consequence on growth. However, a comparison of transcription and translation speeds shows that the synthesis of rRNA is far more rapid. *E. coli*, for example, harbors three rRNAs species per ribosome (5S, 16S, and 23S) with a sum total length of 4566 nucleotides (nt). With a transcription speed of ≈ 40 nt/s a single RNAP needs only $\approx$115 seconds to synthesize these rRNAs. Given that an RNAP contains $\approx$ 4100 AA (significantly less than a ribosome, $m_{Rb} = 7459$ AA), the synthesis of required RNAP does not require a large pool of resources compared to what is required to synthesize the ribosomal proteins. In the following, we extend this logic and calculate the required allocation of ribosomes towards the synthesis of ribosomal proteins and rRNA synthesizing RNAP.

To most clearly introduce the logic of the calculations, we present here only a hypothetical scenario in which precursor supply is unlimited and cells do not have to synthesize metabolic proteins but only consist of ribosomes, rRNA, and the

RNAP required to synthesize rRNA. However, similar calculations can be performed when considering the full allocation model and the metabolic proteins required to supply precursors. The mass of (ribosomal) proteins M_{Rb} is proportional to the total number of ribosomes and depends on their elongation rate γ_{max}, which we assume in this hypothetical scenario to be always maximal. As we are only considering a cell with ribosomal and RNAP proteins, we can state that a certain fraction of the ribosomes ϕ_{Rb} are synthesizing ribosomal proteins whereas the rest $1-\phi_{Rb}$ are generating RNAP. Mathematically, we can enumerate these dynamics as

$$\frac{dM_{Rb}}{dt} = \phi_{Rb}\gamma_{max}M_{Rb}, \tag{S9}$$

for the ribosomal protein biomass dynamics and

$$\frac{dM_{Po}}{dt} = (1-\phi_{Rb})\gamma_{max}M_{Rb}, \tag{S10}$$

for RNAP protein biomass dynamics, where M_{Po} is the total mass of all RNAP.

We consider that all RNAP are synthesizing rRNA to support ribosomal biogenesis, with the amount of rRNA nucleotides depending on the number of RNAP (N_{Po}) and the speed of transcription (v_{tr}),

$$\frac{drRNA}{dt} = v_{tr}N_{Po} \equiv \kappa_{tr}M_{Po}, \tag{S11}$$

where we have defined $\kappa_{tr} \equiv \frac{v_{tr}}{m_{Po}}$ with m_{Po} being the mass of a single RNAP. As ribosomes can only work when a sufficient amount of rRNA is present, we next consider the number of rRNA nucleotides per ribosomal amino acids, $r_{nt} = rRNA/M_{Rb}$. The dynamics is then given by

$$\frac{dr_{nt}}{dt} = \kappa_{tr}\frac{M_{Po}}{M_{Rb}} - r_{nt}\gamma_{max}\phi_{Rb}. \tag{S12}$$

In steady-state growth ($dr_{nt}/dt = 0$ and $\frac{M_{Po}}{M_{Rb}} = \frac{1-\phi_{Rb}}{\phi_{Rb}}$) one obtains a quadratic equation for the fraction ϕ_{Rb} with the solution:

$$\phi_{Rb} = \frac{\kappa_{tr}}{(2r_{nt}\gamma_{max})}\left(-1 \pm \sqrt{1+\frac{4r_{nt}\gamma_{max}}{\kappa_{tr}}}\right) \tag{S13}$$

For a ribosome to function, rRNA nucleotides and amino acids need to be present at a specific ratio, $r_{nt} = rRNA/m_{Rb}$. Taking this ratio and the known rates of transcription and translation, we can estimate the fraction ϕ_{Rb} for *E. coli* yielding $\phi_{Rb} \approx 0.90$. This indicates that only $\approx 10\%$ of the total ribosome pool are needed for RNAP synthesis. It then follows that the upper bound of the growth rate considering the requirements of rRNA synthesis, $\lambda = \gamma(\phi_{Rb,tot} - \phi_{Rb\rightarrow RNAP})$, is different from the exclusively proteinaceous growth rate $\gamma\phi_{Rb}$ by only 10%.

5 Precursors concentrations and the importance of dilution by cell growth

In the main text, we consider that the translation rate γ is dependent on the concentration of precursors c_{pc}. The tug-of-war between the metabolic processes (synthesizing precursors) and protein synthetic processes (consuming precursors) is what determines this value. With the protein density of cells being approximately constant (Supplementary Text 2), we consider the precursors concentration as the mass of precursors per total protein mass, c_{pc}. We describe the dynamics of this precursor concentration c_{pc} as

$$\frac{dc_{pc}}{dt} = \nu(c_{nt})\frac{M_{Mb}}{M} - \gamma(c_{pc})\frac{M_{Rb}}{M} - \underbrace{c_{pc}\gamma(c_{pc})\frac{M_{Rb}}{M}}_{\text{dilution}}, \tag{S14}$$

where M, M_{Mb}, and M_{Rb} denote the masses of the total protein, metabolic protein, and ribosomal protein pools, respectively. The latter term in the above equation denotes the decrease in the precursor concentration due to the increase in biomass – i.e., this term considers the decrease in precursor concentration due to dilution upon a growing cell volume. Through a change-of-variables from m_{pc} to c_{pc}, it mathematically follows that

$$\frac{dc_{pc}}{dt} = \frac{d}{dt}\left(\frac{M_{pc}}{M}\right) = \frac{1}{M}\frac{dM_{pc}}{dt} - \underbrace{c_{pc}\frac{1}{M}\frac{dM}{dt}}_{\text{dilution}}. \tag{S15}$$

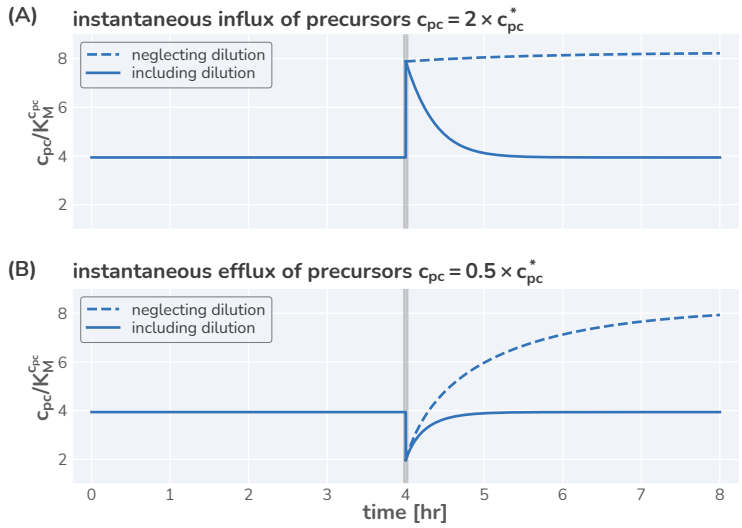

Figure S1: Neglecting effect of precursor dilution results in an unstable steady-state. Integrated dynamics of the model equations including (solid lines) and neglecting (dashed lines) the dilution of the precursors with increasing biomass. At time $t = 4$ hr (gray vertical line), the precursor concentration is instantaneous increased (A) or decreased (B) by a factor of 2 and the system is allowed to respond. Neglecting the effect of dilution results in a monotonic increase in the precursor concentration whereas including dilution allows a rapid return to the steady-state concentration.

In many previous allocation models (outlined in Sec. 1) it is assumed that the effect of dilution is negligible compared to the magnitude of metabolism and protein synthesis [10, 13, 24]. We contend, however, that the effect of dilution is *not* negligible when one considers the *difference* between the metabolic and translational processes. At steady-state, Eq. S14 equates to zero, which upon some rearrangement yields

$$\nu(c_{nt})\phi_{Mb} - \gamma(c_{pc})\phi_{Rb} = c_{pc}\gamma(c_{pc})\phi_{Rb}. \tag{S16}$$

where we note at steady-state $\frac{M_{Rb}}{M} = \phi_{Rb}$ and $\frac{M_{Mb}}{M} = \phi_{Mb}$. When the effect of dilution is neglected (i.e. setting the right-hand-side of Eq. S16 equal to 0), it is required that steady-state is only reached when the two fluxes are equal. Thus, if there is any perturbation to the precursor concentration, such as a sudden influx [Fig. S1(A)] or efflux [Fig. S1(B)] of precursors, the system has no recourse to re-establish a steady-state (dashed lines in Fig. S1). In the case where the effect of dilution is not neglected, the system relaxes back to the stable steady-state (solid lines in Fig. S1) as the influence of dilution increases or decreases in response to the change in precursor concentration.

To obtain biologically relevant analytical solutions we thus explicitly include the dilution factor. Notably, keeping the dilution term around is also what allows analytical solutions to be derived. In previous works [10, 24], it was necessary to include end-product inhibition as a regulatory element of the metabolic flux, one which we do not need to consider here. In mathematical terms, no additional parameters need to be included to define a dependence of the metabolic rate on the precursor concentration As such, the emergence of a steady-state is less of a mystery: it does not require the integration of complex regulation schemes but readily emerges in steady environmental conditions and when the allocation of protein synthesis is constant.

6 Derivation of Analytical Expressions

In the main text, we present several analytical relations pertinent to steady-state growth. These relations follow from the simple allocation model (see Sec. 11 for a discussion of the flux-parity model) and describe (i) how the growth rate depends on model parameters (Fig. 2C) and (ii) how ribosome content depends on other model parameters for the three different regulation scenarios we discuss (Fig. 3D). Here, we introduce a step-by-step derivation of these expressions.

6.1 Deriving the Steady-State Growth Rate

We begin with deriving an expression for the steady-state growth rate λ. As discussed in the main text, steady-state conditions are satisfied when two conditions are met. First, the dynamics of the precursor concentration is constant (i.e. $\frac{dc_{pc}}{dt} = 0$) and the composition of the proteome matches the allocation parameters (i.e. $\frac{M_{Rb}}{M} = \phi_{Rb}$ and $\frac{M_{Mb}}{M} = \phi_{Mb}$).

Furthermore, we assume that in steady-state growth, the concentration of nutrients in the environment is saturating ($c_{nt} \gg K_M^{c_{nt}}$), meaning that $\nu(c_{nt}) \approx \nu_{max}$. With these conditions satisfied, we can rewrite Eq. 5 of the main text as

$$\frac{dc_{pc}}{dt} = \nu_{max}\phi_{Mb} - \gamma(c_{pc}^*)\phi_{Rb} - c_{pc}\gamma(c_{pc}^*)\phi_{Rb} = 0, \tag{S17}$$

where c_{pc}^* is the steady-state precursor concentration.

Noting that in steady-state conditions, the total biomass increases exponentially at a rate $\lambda \equiv \gamma(c_{pc})\phi_{Rb}$, Eq. S17 can be simplified to

$$\frac{dc_{pc}}{dt} = \nu_{max}\phi_{Mb} - \lambda(1 + c_{pc}) = 0. \tag{S18}$$

We can therefore solve for the steady-state precursor concentration c_{pc}^* to yield

$$c_{pc}^* = \frac{\nu_{max}\phi_{Mb}}{\lambda} - 1. \tag{S19}$$

Assuming a Michaelis-Menten form for the translation rate $\gamma(c_{pc}^*)$, we can now define it as a function of the growth rate λ as

$$\gamma(c_{pc}^*) = \frac{\gamma_{max}}{1 + \frac{K_M^{c_{pc}}}{c_{pc}}} = \frac{\gamma_{max}}{1 + \frac{K_M^{c_{pc}}\lambda}{\nu_{max}\phi_{Mb} - \lambda}}. \tag{S20}$$

Knowing that the growth rate $\lambda \equiv \gamma(c_{pc^*})\phi_{Rb}$, and $\phi_{Mb} = 1 - \phi_{Rb} - \phi_O$, we say that

$$\lambda = \frac{\gamma_{max}\phi_{Rb}}{1 + \frac{K_M^{c_{pc}}\lambda}{\nu_{max}(1 - \phi_{Rb} - \phi_O) - \lambda}}. \tag{S21}$$

This can be algebraically manipulated to yield a quadratic equation of the form

$$\lambda^2\left(1 - K_M^{c_{pc}}\right) + \lambda\left(\nu_{max}(1 - \phi_{Rb} - \phi_O) + \gamma_{max}\phi_{Rb}\right) - \gamma_{max}\phi_{Rb}\nu_{max}(1 - \phi_{Rb} - \phi_{Mb}) = 0, \tag{S22}$$

which has one positive root of

$$\lambda = \frac{\nu_{max}(1 - \phi_{Rb} - \phi_O) + \gamma_{max}\phi_{Rb} - \sqrt{(\nu_{max}(1 - \phi_{Rb} - \phi_O) + \gamma_{max}\phi_{Rb})^2 - 4(1 - K_M^{c_{pc}})\gamma_{max}\phi_{Rb}\nu_{max}(1 - \phi_{Rb} - \phi_O)}}{2\left(1 - K_M^{c_{pc}}\right)}. \tag{S23}$$

For notational simplicity, we can define the maximum metabolic output and the maximum translational output as $\mathrm{N} = \nu_{max}(1 - \phi_{Rb} - \phi_O)$ and $\Gamma = \gamma_{max}\phi_{Rb}$, respectively, and substitute them into Eq. S23 to generate

$$\lambda = \frac{\mathrm{N} + \Gamma - \sqrt{(\mathrm{N} + \Gamma)^2 - 4\left(1 - K_M^{c_{pc}}\right)\mathrm{N}\Gamma}}{2\left(1 - K_M^{c_{pc}}\right)}, \tag{S24}$$

which is the equation presented in Fig. 3 of the main text.

6.2 Defining ϕ_{Rb} For Scenarios II and III

In the main text, we provide a description of three plausible regulatory scenarios microbes may employ to regulate their ribosomal content. In Fig. 2 we provide the analytical forms describing these scenarios. Scenario I assumes just a constant, arbitrary allocation parameter $\phi_{Rb} \in [0, 1 - \phi_O]$. Here, we provide a short derivation for the more complicated relations describing ribosomal content under scenarios II and III.

6.2.1 Scenario II: Constant Translation Rate

The second regulatory scenario assumes that the ribosomal content is adjusted to maintain a specific standing concentration of precursors, which we denote as c_{pc}^*. Noting that the growth rate $\lambda \equiv \gamma(c_{pc}^*)\phi_{Rb}$, we can restate Eq. S19 in the form

$$c_{pc}^* = \frac{\nu_{max}(1 - \phi_O - \phi_{Rb})(c_{pc}^* + K_M^{c_{pc}})}{c_{pc}^*\gamma_{max}\phi_{Rb}}. \tag{S25}$$

Some algebraic rearrangement allows us to solve for ϕ_{Rb}, yielding

$$\phi_{Rb} = \frac{(1-\phi_O)\nu_{max}\left(c_{pc}^* + K_M^{c_{pc}}\right)}{\nu_{max}\left(c_{pc}^* + K_M^{c_{pc}}\right) + \gamma_{max}c_{pc}^*\left(c_{pc}^* + 1\right)}. \tag{S26}$$

This expression is equivalent to that shown for scenario II in Fig. 3 of the main text. In evaluating this scenario, we considered the regime in which precursors were in abundance, meaning $c_{pc}^* \gg K_M^{c_{pc}^*}$. Under this regime, Eq. S26 simplifies further to

$$\phi_{Rb} \approx \frac{(1-\phi_O)\nu_{max}}{\gamma_{max}\left(c_{pc}^* + 1\right) + \nu_{max}}. \tag{S27}$$

This represents a strategy where the cell adjusts ϕ_{Rb} to maintain a translation rate very close to γ_{max}.

6.2.2 Scenario III: Optimal Allocation

In this work, we define the optimal allocation of ribosomes ϕ_{Rb} to be that which maximizes the growth rate in a given environment and at a given metabolic state. To determine the optimal ϕ_{Rb}, we can differentiate Eq. S23 with respect to ϕ_{Rb} to yield the cumbersome expression

$$\frac{\partial\lambda}{\partial\phi_{Rb}} = \frac{1}{2\left(1+K_M^{c_{pc}}\right)}\times \tag{S28}$$

$$\left[\gamma_{max} - \nu_{max} - \frac{2\gamma_{max}\nu_{max}\left(1-K_M^{c_{pc}}\right)\left(2\phi_{Rb}+\phi_O-1\right) + \left(\gamma_{max}-\nu_{max}\right)\left(\gamma_{max}\phi_{Rb} + \nu_{max}\left(1-\phi_O-\phi_{Rb}\right)\right)}{\sqrt{\left(\gamma_{max}\phi_{Rb} + \nu_{max}\left(1-\phi_O-\phi_{Rb}\right)\right)^2 - 4\left(1-K_M^{c_{pc}}\right)\gamma_{max}\nu_{max}\phi_{Rb}\left(1-\phi_O-\phi_{Rb}\right)}}\right]. \tag{S29}$$

Setting this expression equal to zero and solving for ϕ_{Rb} results in

$$\phi_{Rb} = \frac{(1-\phi_O)\left(\gamma_{max}\nu_{max}\left(1-2K_M^{c_{pc}}\right) + \nu_{max}^2 + \sqrt{K_M^{c_{pc}}\gamma_{max}\nu_{max}}(\gamma_{max}-\nu_{max})\right)}{(\gamma_{max}+\nu_{max})^2 - 4K_M^{c_{pc}}\gamma_{max}\nu_{max}} \tag{S30}$$

which is the optimal allocation towards ribosomes as presented in Fig. 3D of the main text.

7 Additional considerations relevant at slow growth

While the optimal allocation model (scenario III) can describe the observed relation between ribosome abundance and growth rates remarkably well for fast growth, predictions and observations disagree when growth rates fall below $\lambda < 0.5$ hr^{-1} [Fig. 4 (B) and (E) of the main text]. The observed values are higher than what is predicted by the regulation scenarios II (constant translation) and III (optimal allocation) which might be attributed to a range of additional aspects, including (i) the active degradation of proteins, (ii) a comparison with data which has not yet reached steady-state, and (iii) an increase in the fraction of inactive ribosomes at slower growth. Here we discuss these additional aspects and conclude that additional experiments are needed before extending our modeling approach to additionally capture very slow growth conditions.

7.1 Active protein degradation

The active degradation of proteins is an additional factor which might require a higher content of ribosomes than what is predicted by the model at slow growth. In formulating the allocation model, we considered only protein synthesis but not degradation. Mathematically, we modeled the change in protein mass to depend solely on translation,

$$\frac{dM}{dt} = \gamma(c_{pc})M_{Rb}, \tag{S31}$$

but did not include a degradation term, *e.g.*

$$\frac{dM}{dt} = \underbrace{\gamma(c_{pc})M_{Rb}}_{\text{synthesis}} - \underbrace{k_{deg}M}_{\text{degradation}} \tag{S32}$$

This simplification is well justified when growth is fast since observed degradation half-lives are then very long compared to the time-scale of growth. For *E. coli* for example, measured degradation rates k_{deg} remain below 0.02 hr^{-1}, substantially lower than observed growth-rates [25]. However, the timescales become comparable when growth is slow and an explicit consideration of protein degradation is needed. Furthermore, protein degradation rates appear to increase at very slow growth ($k_{degr} \approx 0.03$ hr^{-1} for *E. coli*). For a more detailed discussion of peptide degradation and its possible affect on the ribosome content at slow growth we refer to a recent study from Calabrese *et al.* [26].

7.2 Observations not in steady-state

Another aspect which might explain the derivation between available data and predictions is related to the specifics of the experimental culturing protocols: slow growing cultures may take such a long time to reach steady-state that the experimental measurements may not reflect the steady-state physiology, making an assessment of the model accuracy difficult in this regime. The experimental studies which we use to test our model (listed in Table S2) provide a description of the culturing conditions used, though the specifics of the procedure (such as culturing lengths) are given in broad terms. Most studies relied on a procedure more-or-less as follows.

1. A seeding culture is grown to exponential phase in a rich growth medium (such as LB, $\lambda \approx 2$ hr^{-1}).
2. The seeding culture is diluted into the experimental medium (termed the *preculture*) which is allowed to grow "overnight" (which we take to be between 12 and 18 hours) to mid-exponential phase.
3. The preculture is then modestly diluted into the experimental medium and allowed to grow for one or two doublings (≈ 1.5 generations) before measurements are made.

While this is a robust protocol to ensure that a fast growing cultures reach steady-state, step 2 requires particular care when slow growth conditions are explored. As the seed culture is typically grown in rich media, the inoculum of cells will have a significantly large allocation towards ribosomes, such as $\phi_{Rb} \approx 0.2$ for a culture grown in LB. As the degradation of ribosomes is slow, this "bolus of ribosomes" only decreases via dilution as the culture grows. For example, a poor growth medium which can support a growth rate of $\lambda \approx 0.2$ would require more than 20 hours to reach steady-state within typical measurement errors of 0.1% [Fig. S2(A) and (B)]. Notably, this calculation reflects a best-case scenario where there is no growth arrest upon transfer from from the seeding culture to the preculture medium. In reality, long phases of growth-arrest with lag-times on the order of hours is common [27]. In conclusion, precultures have to maintained for a very long time, of the order of a day, when aiming for a steady-state culture in very poor conditions, substantially longer than what the overnight cultures commonly mentioned in the protocols would support.

To see how a too short preculture time could alter the predictions of our model we numerically integrated the flux-parity model (described in Sec. 11) assuming a seed culture grown in LB with a large initial ribosome content [Fig. S2(C)]. From this analysis, it is plausible that some of the discrepancy between the model predictions and experimental measurements could be explained by harvesting cells before they have reached steady-state. More detailed information would be needed (such as precise preculturing duration) to concretely assess the magnitude of this effect in the dataset we have assembled.

7.3 Inactive ribosomes

Several studies have reported that microbes commonly maintain a pool of inactive ribosomes [19, 28–31]. In slow growth conditions, an inactive ribosome pool may promote quicker recovery once conditions improve, a phenomenon sometimes called a "spare ribosome capacity" [29, 32, 33]. In our model, we do not consider an inactive pool of ribosomes – rather, we assume that *all* ribosomes are active. This simplification might thus explain the derivation between the observed ribosomal content in cells and the model predictions. However, direct evidence which supports the maintenance of an inactive ribosome fraction is sparse and many open questions remain. Here we summarize our perspective.

To thrive in fluctuating conditions, cells have to be capable to dynamically regulate the activity of ribosomes. For example, consider a strong downshift scenario where cells transition abruptly from very fast growth (supported by a high precursor flux) to very slow growth (supported by a much lower precursor flux). During the shift, a substantial fraction of the ribosomes needs to be immediately inactivated to avoid exhaustion of the remaining precursor pool leading to cessation of protein synthesis. Molecular studies have supported this hypothesis as proteins which trigger ribosome inactivation

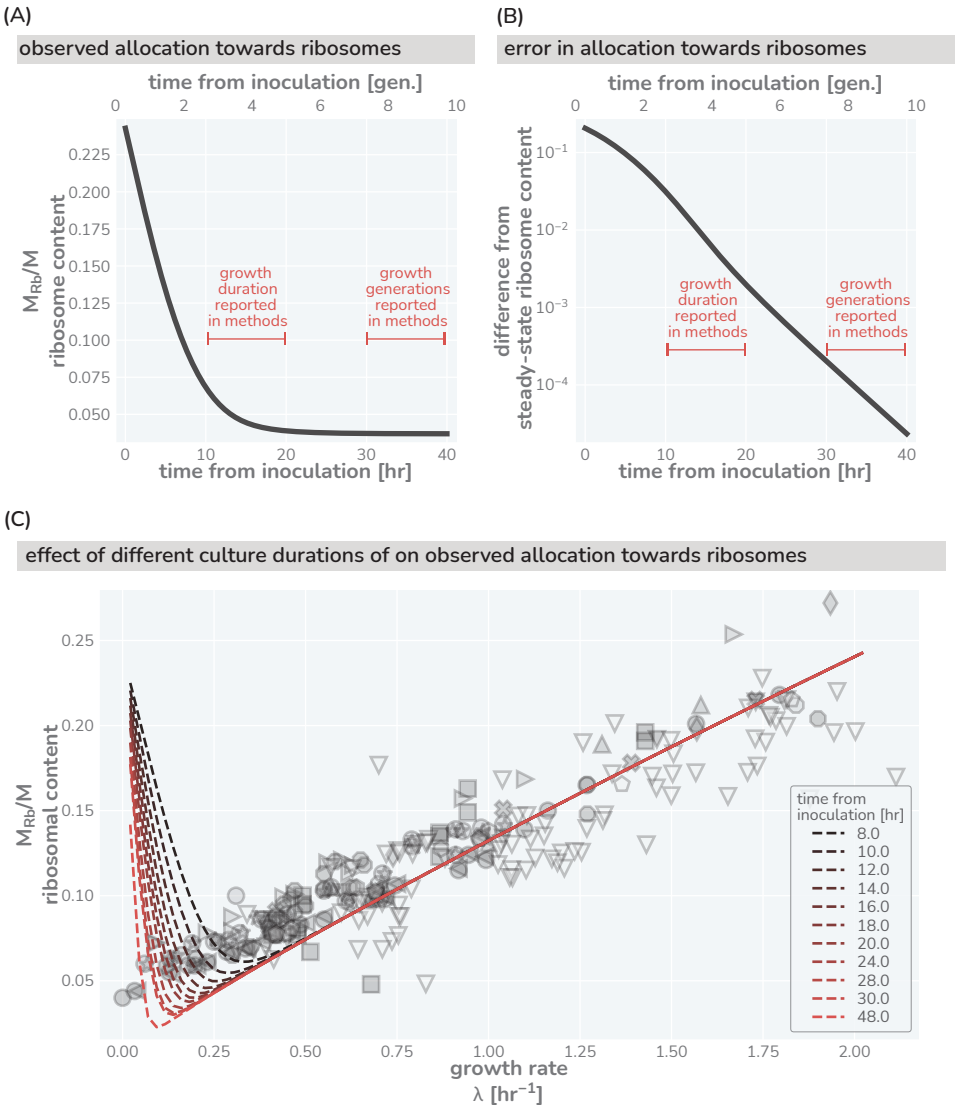

Figure S2: Effect of culturing time on observed ribosomal content at slow growth. (A) Predicted dynamics of equilibration to steady-state from a seeding culture with high ribosome content ($\phi_{Rb} \approx 0.25$, $\lambda \approx 2.0$ hr^{-1}, $\nu_{max} \approx 11$ hr^{-1}) into a poor growth medium with a low steady-state ribosome content ($\phi_{Rb} \approx 0.03$, $\lambda \approx 0.2$ hr^{-1}, $\nu_{max} \approx 0.03$ hr^{-1}). (B) The difference between the measurable ribosomal content and the steady-state value in the poor growth medium. Red brackets in (A) and (B) correspond to claimed culturing duration commonly seen in the literature. Culturing time of "overnight" is taken to approximately mean 12 hours. (C) The effect of insufficient culturing time on the measurable ribosome content. Red dashed lines show model predictions assuming a seeding culture with same parameters as in (A) and (B) into different media with a range of metabolic rates. Dark to light colors correspond to short (8 hr) and long (48 hr) culturing conditions, respectively. Data and markers are the same as those shown in Fig. 4 of the main text.

(termed "hibernation factors") are synthesized relatively quickly to the downshift. *E. coli*, for example, uses ribosome modulation factor (RMF) among others which dimerizes ribosomes forming an inactive 100s complex [34]. Transcriptomic analysis has further show that RMF is heavily expressed during a downshift or during entry into starvation, confirming that cells can quickly change the fraction of active ribosomes. However, while we believe in the important role of ribosome inactivation during downshifts, we also believe that the role of ribosome inactivation during steady-state growth remains much less clear. Given our current experimental knowledge, we challenge the idea that cells actively maintain a large fraction of inactive ribosomes during slow growth to be prepared for a quick growth recovery once growth conditions resume. This view of "spare capacity" is based on the reported large fraction of inactive ribosomes during growth in poor growth conditions (growth rate $\lambda \leq 0.5$ hr^{-1}). We see two problems with the derivation of this picture. First, while anticipatory behavior sounds plausible given the reported high fraction of inactive ribosomes, we should keep in mind that the fraction of inactive ribosomes is not based on direct experimental measurements. Instead, the fraction is commonly estimated by the difference between observed growth and measured translation rates [28], which assumes that measured translation rates correctly reflect the average translation rate of all active ribosomes. More direct measurements of active fractions are possible in principle, such as by ribosome or polysome profiling, but very hard to perform in practice with quantitative accuracy. Secondly, this view assumes that cultures have reached a steady-state when the fraction of inactive ribosomes is estimated. As is discussed in Sec. 5, the time required for cultures to reach steady-state is particularly long for poor growth conditions; for growth rates $\lambda < 0.5$ hr^{-1}, the times cultures need to spend in pre-culture states extend substantially beyond the 15 to 20 hour periods commonly used for overnight precultures. There is thus the possibility that reported inactive ribosomes in slow growth conditions are high because cultures are still adjusting to the encountered growth conditions, rather than being high because cells actively maintain a high fraction of inactive ribosomes during slow growth in steady conditions.

In conclusion, a quite involved combination of aspects might be at play at slow growth and we thus did not expand our model to better cover slow growth observations and explicitly include active protein digestion and inactive ribosomes. Further studies at both the experimental and theoretical level are needed to fully assess the role of inactive ribosomes in steady-state growth.

8 What makes the fraction of "other" proteins?

In the specification of the simple ribosomal allocation model, we asserted that the entire proteome could be categorized into just three sectors – one for metabolic proteins, one for ribosomal proteins, and one for all "other" proteins. In this section, we demonstrate that the precise value of ϕ_O, the allocation parameter describing the synthesis of other proteins, is largely independent in predicting growth dynamics and we explore the experimental evidence which establishes and quantify this sector in *E. coli*.

8.1 Defining the other proteins

In this work, we assign one sector of the proteome to be composed of ribosomal proteins. This sector is well defined and specifically contains the ≈ 50 proteins that make up the 50S and 30S subunits of the ribosome. It is more difficult, however, to determine what proteins are "metabolic" and which should be classified as "others". The past decade has seen a flurry of studies leveraging modern proteomic methods to measure the abundances and relative concentrations of the thousands of protein species which constitute bacterial cells [35–39]. Schmidt *et al.* [37], for example, measured the absolute abundances of 2041 individual proteins in *E. coli* across 22 growth conditions. This data set, coupled with the mountain of functional annotation available for *E. coli* [40] allows us to explore how different biological processes scale with the steady-state growth rate.

One method to do so is through Clusters of Orthologous Groups (COGs) [41], which groups genes by their annotated functions into distinct "classes" of proteins. Fig. S3(A) shows the protein sector mass fraction for all proteins involved in ribosomal structure and biogenesis (gold; COG class J), general metabolism (purple; COG classes P, H, F, E, G, C), and all other processes (black; COG classes X, O, U, W, Z, N, M, T, V, Y, D, B, L, K, A, R, S). Exploring how the mass fractions of these very general annotations scale with growth rate reveals a strong anticorrelation between ribosomal and metabolic genes, with an approximate constant fraction of "other" proteins. One approach is to rely on this annotation to determine the magnitude of the allocation towards other proteins and take $\phi_O \approx 0.3$.

An alternative approach is to determine how the abundance of each individual protein changes with the steady-state growth rate. For each protein in the data of Schmidt *et al.*, we computed the Pearson correlation coefficient between the proteome mass fraction of each individual protein and the growth rate with Pearson's r values of -1.0 and 1.0 showing perfect anticorrelation and correlation, respectively. With a measure of the correlation, we made the somewhat arbitrary decision that any protein with a Pearson's r between $-0.5 < r < 0.5$ to be classified as "constant", having weak or

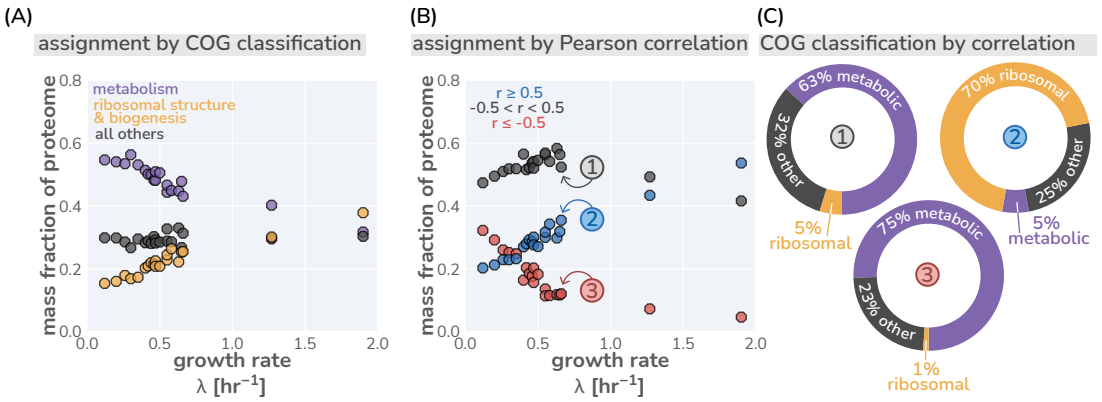

Figure S3: Different classification strategies of "other" proteins. (A) Classification of proteins in mass spectrometry data (Schmidt et al., 2016 [37]) by their COG classification. 'Metabolism' includes all transport and metabolic processes (COG letters: P,H,F,E,G,C [41]). (B) Classification of "other" proteins by their growth-rate dependence. Other proteins are defined as those with a Pearson correlation coefficient between -0.5 and +0.5. (C) The composition of each correlation-defined sector for one condition are shown as doughnut plots. Colors correspond to the COG classifications shown in (A) and circled numbers correspond to labeled points in (B).

no correlation with the growth rate at all. Fig. S3(B) shows the results of this classification. Here, it appears that the constant (black points) sector hovers around a mass fraction of ≈ 0.5, another candidate value for ϕ_O. To see if this classification scheme was reasonable, we examined what COG classes were represented in each sector defined by the Pearson correlation. Fig. S3(C) shows a representative breakdown of each sector by the same COG classification as used in (A). Here, it becomes clear that metabolic proteins dominate both the "constant" and "negatively-correlated" classes whereas the "positively-correlated" sector contains predominantly ribosomal proteins. This illustrates that there exists a sizeable pool of proteins whose relative abundance is largely independent of growth rate, despite their classification as being involved in metabolism.

This exploration highlights a subtle yet important point in the classification of the proteome into sectors. While in the main text we specify proteins as being *involved* in metabolism or protein synthesis, we really mean that they can be classified as having a dependence on the growth rate, whether it be positive or negative. Hui and colleagues [42] recently explored in great depth how the *E. coli* proteome can be broken into six or seven sectors which have different correlations with the growth rate under different types of limitation. In this work, they arrived at an estimation that approximately one-half of the proteome is growth rate independent ($\phi_O = 0.55$) under the many conditions they examined. This value agrees with the simple growth-correlation classification presented above and we thus taken here $\phi_O = 0.55$ for *E. coli*. However, as we describe in the following section, the predictions made by our model is largely independent on the precise value of this parameter.

8.2 Neglecting the other proteins

In Eq. 7 of the main text, we define the mass dynamics of the protein sectors (M_{Rb}, M_{Mb}, and M_O) as

$$\frac{dM_{Rb}}{M} = \phi_{Rb}\frac{dM}{dt}\ ;\ \frac{dM_{Mb}}{dt} = \phi_{Mb}\frac{dM}{dt}\ ;\ \frac{dM_O}{dt} = \phi_O\frac{dM}{dt}, \tag{S33}$$

where ϕ_{Rb}, ϕ_{Mb}, and ϕ_O denote allocation parameters for ribosomal, metabolic, and "other" proteins, respectively. We further introduce the constraint that these three classes make up the entire composition of the proteome, meaning that

$$\phi_O + \phi_{Rb} + \phi_{Mb} = 1. \tag{S34}$$

As the majority of the predictions of this work are dependent on the allocation towards ribosomes, we can alternatively define the metabolic allocation factor given Eq. S34 as

$$\phi_{Mb} = 1 - \phi_{Rb} - \phi_O. \tag{S35}$$

Thus, so long as the values of ϕ_{Rb} and ϕ_O are known, the value of ϕ_{Mb} follows and thus the maximal metabolic output N can be defined as

$$\mathrm{N} = \nu_{max}\phi_{Mb} = \nu_{max}\left(1 - \phi_{Rb} - \phi_O\right), \tag{S36}$$

where ν_{max} is the maximum metabolic rate for that particular condition and composition of the metabolic sector. However, suppose we *didn't* know the value of ϕ_O and *only* knew ϕ_{Rb}. In this case, we could further reduce the dimensionality of

the proteome by stating that all of the proteins are either ribosomal or are *not* ribosomal. In this case, the allocation parameters for this scenario become

$$\phi^*_{Mb} + \phi_{Rb} = 1 \; ; \; \phi^*_{Mb} = 1 - \phi_{Rb}, \tag{S37}$$

where the new metabolic allocation parameter includes an unknown "other" allocation such that

$$\phi^*_{Mb} = \phi_{Mb} + \phi_O. \tag{S38}$$

It then follows that the maximal metabolic output given this allocation N^* is calculated as

$$\mathrm{N}^* = \nu^*_{max}\phi^*_{Mb} = \nu^*_{max}\left(1 - \phi_{Rb}\right). \tag{S39}$$

This structuring implies that the metabolic outputs are different whether one knows ϕ_O or not. However, these two scenarios can be made equivalent by a simple rescaling of the metabolic rate ν_{max}. Setting Eq. S36 and Eq. S39 to be equivalent and solving for the metabolic rate ν_{max} where ϕ_O is known yields

$$\nu_{max} = \frac{\nu^*_{max}\left(1 - \phi_{Rb}\right)}{\left(1 - \phi_O - \phi_{Rb}\right)}. \tag{S40}$$

Thus, one can achieve quantitatively identical predictions between the scenario where ϕ_O is known and that where ϕ_O is unknown by a simple rescaling of the metabolic rate, ν_{max}. While this serves as a contrived example, it reveals that our estimation of ϕ_O having a constant allocation $\phi_O = 0.55$, as has been inferred from mass spectrometry studies [42] (see previous paragraph), to be largely inconsequential for the predictions made in this work. However, there are some scenarios where the precise value of ϕ_O *does* become important (such as in the case of excess protein stress), which are discussed in Sec. 11.

9 Inactive ribosomes are not needed to describe the linear relation between ribosome content and growth rate

In their simplest form, allocation considerations assume cells optimally control ribosome content such that protein synthesis by ribosomes occurs with a fixed translation speed or rate (γ_0). To have all ribosomes working with a constant rate, the allocation parameter ϕ_{Rb} controlling the fraction of ribosomes in the cell must then scale linearly with the growth rate, $\phi_R = \gamma_0\lambda$. This relation does not have an offset: At the extreme limit where metabolic proteins are hardly supporting any growth ($\lambda \to 0$), this linear scaling implies that the ribosome content drops to zero ($\phi_{Rb} \to 0$). However, this notion appears to disagree with experimental observations. When a linear regression is performed on the ribosomal content data (solid line in Fig. S4) as has been done in other studies [11], one yields an "offset", $\phi^{(min)}_{Rb}$, yielding a linear relation of

$$\phi_{Rb} = \phi^{(min)}_{Rb} + \gamma_0\lambda. \tag{S41}$$

Previous phenomenological studies have thus rationalized this offset as a growth-rate independent abundance of inactive ribosomes which are not involved in translation [11, 32]. However, later measurements have confirmed that the translation rate is decidedly *not* constant and in fact increases with the growth rate, asymptotically approaching a maximal value [28]. In Dai *et al.*, 2016 [28], the authors use this observation to hypothesize that most of the ribosomes remains active as long as growth rates are not slow ($\lambda \geq 0.5$ hr^{-1}). Consistent with this idea, our rendering of the optimal allocation model (scenario III in the main text) explains why this offset emerges from a linear regression without the introduction of any inactive ribosomes.

The strong correlation between the ribosomal content and bulk growth rate has long been hailed as a linear relation, however there is no *a priori* rationale behind stating it must be linear. In fact, our optimal allocation model results in a *non-linear*, yet still monotonically positive, correlation between the ribosomal content and the growth rate. While non-linear, it is approximately linear in the regime of fast growth, $\lambda \geq 0.5$ hr^{-1}. Extending this approximately linear behavior yields a slope and an offset (dashed line in Fig. S4) which is comparable to the empirically observed offset.

The fundamental reason for this observation is that a close-to-maximal translation rate requires very high precursor concentrations which are very resource demanding to sustain. In our model, this is described by a translation rate which is only met when the precursor concentrations c_{pc} are substantially higher than the Michaelis-Menten constant $K_M^{c_{pc}}$. These dependence can be further explored via the interactive versions of the manuscript figures at our paper website.

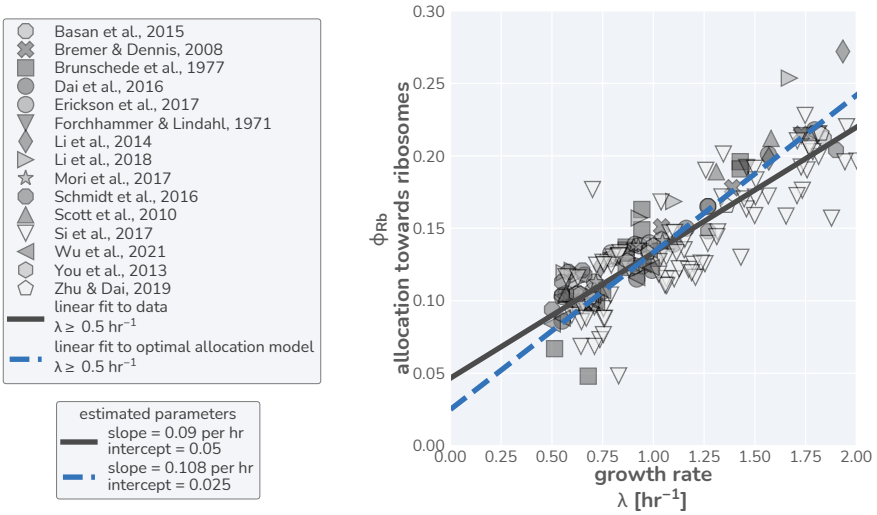

Figure S4: Linear regression on data and optimal allocation model in fast-growth regime yields comparable offsets. Data in right-hand panel corresponds to the same measurements used in the main text but restricted to only those data where the growth rate is $\lambda \geq 0.5$ hr^{-1}. A simple linear regression (using the SciPy python library) was performed on this data (solid black line) to yield a slope of ≈ 0.1 hr^{-1} and an intercept of $\phi_{Rb}^{(min)} \approx 0.05$, in line with parameter estimates from previous work [11]. Restricting the model predictions to growth rates $\lambda \geq 0.5$ hr^{-1} yields a linear relation (dashed blue line) with a slope of ≈ 0.1 hr^{-1} and an intercept of $\phi_{Rb}^{(min)} \approx 0.02$.

10 Application of the Model to *Saccharomyces cerevisiae*

In the main text, we evaluated the model predictions by direct comparison with observations for *E. coli*, as appropriate data for this model organism is highly abundant. However, the model predictions should be applicable more broadly to any microbial organism whose growth rate is primarily dependent on the synthesis of protein biomass. The budding yeast *S. cerevisiae* is one such microbe where our approach may be applied and used to quantitatively explore aspects of eukaryotic microbial physiology, and we here provide a parameterization of our model.

We first surveyed the literature to identify and assign *a priori* values to the major model parameters, which are listed in Table S3. Of particular note is the substantial difference between *E. coli* and *S. cerevisiae* in the proteinaceous mass of a single ribosome ($m_{Rb} = 7459$ AA and $m_{Rb} = 11984$ AA, respectively) and the reported maximum translation speed ($v_{tl,max} \approx 20$ AA/s and $v_{tl,max} \approx 10$ AA/s, respectively) which lead to a substantial difference in the maximum translation rates ($\gamma_{max} = v_{tl,max}/m_{Rb}$). We further note that the fraction of the proteome occupied by the "other" protein class has not received sufficient characterization in yeast. However, this is not of relevance when comparing model predictions and data during steady-state growth as a variation of ϕ_0 merely leads to a rescaling of the maximum metabolic rate ν_{max} which we vary anyway to scan growth rates (see Sec. 8).

To evaluate the applicability of our model, we further explored the *S. cerevisiae* literature for basic physiological measurements including ribosomal content and translation speeds across growth conditions. To our surprise, we found that these fundamental physiological quantities have been scarcely measured, despite *S. cerevisiae* being a heavily characterized model organism. This is true particularly for the translation speed, for which there are only four or five reported measurements. Nevertheless, we assembled a collated data set from 10 independent studies that we were able to find and appropriately vet and compared their values to the model predictions (Table S4).

Specifically, we evaluated the regulatory scenarios II and III in which the translation rate is either held constant at $\approx 90\%$ of its maximum value or the allocation towards ribosomes is tuned such that growth rate is optimized (Fig. S5). While the paucity of the data precludes us from making any concrete assessments, it is plausible that *S. cerevisiae* also follows an scheme of optimal regulation of ribosomal allocation (scenario III, blue line). More study is needed, particularly of the growth-rate dependence of translation speed, to evaluate the applicability of this approach to yeast.

11 Implementing Flux-Parity Regulation via ppGpp

In the main text, we presented in broad strokes a model of flux-parity regulation utilizing ppGpp. Here, we expand upon this description and provide a full formulation of the underlying mathematics, explore its dependence on parameter values, and demonstrate how it can describe non steady-state growth and accommodate physiological perturbations.

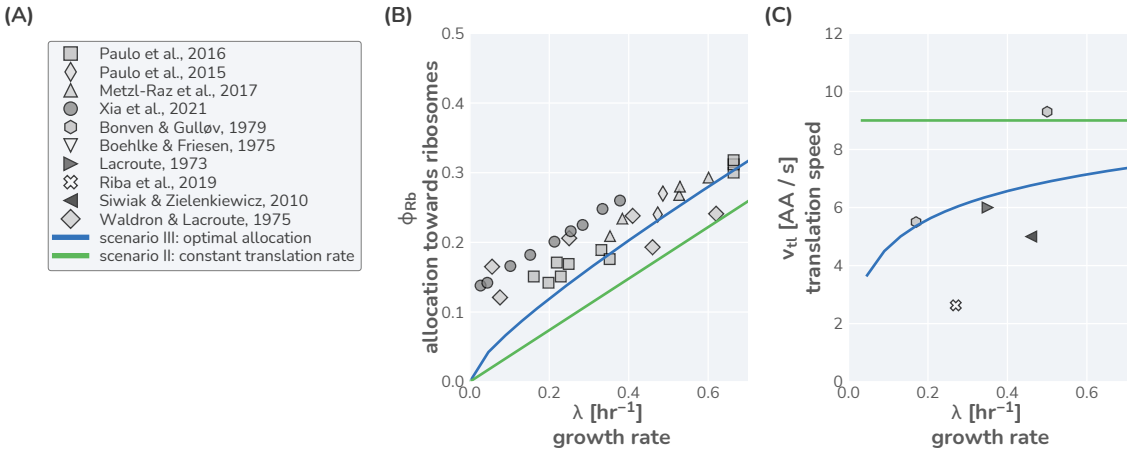

Figure S5: Comparison of model predictions to data from Saccharomyces cerevisiae. (A) List of literature sources reporting measurement of ribosomal content and/or translation speed measurements. Experimental data for (B) ribosomal content and (C) translation speed are shown as function of growth rate. Green and blue lines correspond to model predictions for scenario II and III, respectively, using the model parameters defined in Table S3. For scenario II, a constant translation rate of 90% of $v_{tl,max}$ was used.

11.1 Formulation of model

To include ppGpp signaling into the ribosomal allocation model, we must perform two tasks. First, we must explicitly model the dynamics of both charged- and uncharged-tRNAs. Secondly, we must tie the relative abundances of these tRNAs to the allocation parameters such that when charged-tRNAs are limiting and uncharged-tRNAs in abundance, the system reacts by adjusting the allocation parameters towards ribosomal proteins and away from metabolic proteins (ϕ_{Rb} and ϕ_{Mb}).

We consider there to be two pools of tRNAs – those charged with an amino acid (denoted as $tRNA^*$) and those that are uncharged ($tRNA$). Rather than keeping track of the copy numbers of these tRNAs, we instead model their concentration as relative mass abundances (relative to the total protein biomass M, see Sec. 2), treating each tRNA to have an effective mass of one amino acid as each tRNA can in principle be charged. Much as in the main text, we can model the concentration dynamics of these pools of tRNAs by considering three processes – the generation of the tRNAs, the consumption of the tRNAs, and the effect of dilution as the biomass grows.

We begin first with modeling the dynamics of the charged-tRNA pool, $tRNA^*$. Here, we consider that charged-tRNAs are synthesized from one free amino acid and one uncharged-tRNA and further assume that the pool of free amino acids is abundant enough such that the tRNA pool is the rate limiting component. Making this assumption allows us to state that the conversion of one uncharged-tRNA to one charged-tRNA via the metabolic machinery proceeds at a rate $\nu(tRNA)$, itself dependent on the *uncharged-tRNA* concentration. Likewise, we consider that the conversion of one charged-tRNA to an uncharged-tRNA is only possible via protein synthesis, which proceeds at a rate $\gamma(tRNA^*)$ that is dependent on the *charged-tRNA* concentration. Finally, as is discussed in Sec. 5 of this supplement and in the main text, we must also consider how the mere fact of growing biomass effectively dilutes the charged-tRNA concentration. Together, these processes can be combined to enumerate the dynamics of the charged-tRNA pool as

$$\frac{dtRNA^*}{dt} = \overbrace{\frac{\nu(tRNA)M_{Mb}}{M}}^{\text{generation via metabolism}} - \underbrace{\frac{\gamma(tRNA^*)M_{Rb}}{M}}_{\text{consumption via protein synthesis}} - \overbrace{\frac{tRNA^*\gamma(tRNA^*)M_{Rb}}{M}}^{\text{reduction via dilution}}. \tag{S42}$$

The dynamics for the pool of uncharged-tRNAs can be constructed in a similar manner, with the caveat that the generation of new uncharged-tRNAs occurs from both protein synthesis (converting one charged-tRNA into one uncharged-tRNA) and from transcription of the individual tRNA genes. We consider the latter to occur at a rate κ, which has dimensions of concentration per unit time. Using the same logic of mapping the productive and consumptive processes, we

can enumerate the dynamics of the uncharged-tRNA pool as

$$\frac{dtRNA}{dt} = \overbrace{\kappa}^{\text{production via transcription}} + \underbrace{\frac{\gamma(tRNA^*)M_{Rb}}{M}}_{\text{occurance via protein synthesis}} - \overbrace{\frac{\nu(tRNA)M_{Mb}}{M}}^{\text{consumption via metabolism}} - \underbrace{\frac{tRNA\gamma(tRNA^*)M_{Rb}}{M}}_{\text{reduction via dilution}}. \tag{S43}$$

These expressions comprehensively define the dynamics of the tRNA pool, from generation via transcription to their recycling between charged and uncharged states through metabolic and translational fluxes, respectively. As in the main text, we posit that the dynamics of the ribosomal M_{Rb}, metabolic M_{Mb}, and "other" M_O protein masses follow via the allocation parameters ϕ_{Rb}, ϕ_{Mb}, and ϕ_O respectively. However, in this treatment of the model, we consider these parameters, with the exception of ϕ_O, to be dynamic and depend on the intracellular concentration of ppGpp. Mathematically, we state this as

$$\frac{dM_{Rb}}{dt} = \phi_{Rb}(\text{ppGpp})\frac{dM}{dt}\ ;\ \frac{dM_{Mb}}{dt} = [1-\phi_O-\phi_{Rb}(\text{ppGpp})]\frac{dM}{dt}\ ;\ \frac{dM_O}{dt} = \phi_O\frac{dM}{dt}. \tag{S44}$$

We are now tasked with (i) enumerating the dynamics of ppGpp and (ii) assigning a specific functional form to $\phi_{Rb}(\text{ppGpp})$. The biochemistry of ppGpp synthesis, degradation, and binding to the transcription machinery has been studied in *E. coli* among other prokaryotes, revealing the enzyme(s) important for this process. In *E. coli* RelA and SpoT. Many molecular details revealing how those enzymes control ppGpp levels in response to the abundance of tRNA levels are known but important details also remain puzzling [43, 44]. Thus, while other works consider the dynamics of these specific proteins in more detail [12, 13], we here take a more coarse-grained view. Specifically, we make introduce the ansatz that the dynamics of ppGpp synthesis and degradation are sufficiently fast compared to the timescale of protein synthesis such that it can be treated as being in steady-state instantaneously. Secondly, we take the concentration of ppGpp to be inversely proportional to the relative abundance of charged- to uncharged-tRNAs,

$$\text{ppGpp} \propto \frac{1}{\frac{tRNA^*}{tRNA}}. \tag{S45}$$

This is a well-motivated starting point as in *E. coli*, ppGpp is primarily synthesized via RelA when an uncharged-tRNA enters the A-site of a translating ribosome, forming a stalled complex. As binding of a charged-tRNA or an uncharged-tRNA is a competitive process, the probability of one or the other being bound is dependent on their relative concentrations, rather than the absolute concentrations of either species. However other processes which affect ppGpp levels, including the synthesis and degradation by SpoT in relation to ribosome activity, are less well understood [45]. Accordingly, we consider our approach to describe ppGpp as inversely proportional to the relative abundance of charged- to uncharged-tRNAs rather as a well-motivated ansatz than a fully established biochemical relation.

Given the relation between ppGpp and tRNA charging ratio, (S45), we can now define the allocation towards ribosomes to be a function of the tRNA charging ratio, $\phi_{Rb}\left(\frac{tRNA^*}{tRNA}\right)$. To assign a specific functional form to this relation, we assume that the expression of ribosomal genes is in first order described by a simple binding kinetics of ppGpp to the transcriptional machinery and the allocation towards ribosomes follows a form similar to that of a Michaelis-Menten relation,

$$\phi_{Rb}\left(\frac{tRNA^*}{tRNA}\right) = (1-\phi_O)\frac{\frac{tRNA^*}{tRNA}}{\frac{tRNA^*}{tRNA}+\tau}, \tag{S46}$$

Here, the parameter τ represents the value of the charged- to uncharged-tRNA ratio where ϕ_{Rb} is at its half-maximal value. The maximal value itself depends on the magnitude of ϕ_O, the allocation towards other proteins, which we are considering to be independent of ppGpp; $\phi_{Rb}^{(max)} = 1-\phi_O$.

The transcription of tRNA genes towards novel tRNA synthesis has also been shown to be regulated with ppGpp, appearing to closely match the regulatory behavior of ribosomal proteins [46]. We therefore model that the tRNA synthesis rate κ (introduced in (S43)) is similarly modulated by the charged- to uncharged-tRNA ratio,

$$\kappa\left(\frac{tRNA^*}{tRNA}\right) = \kappa_{\text{max}}\frac{\frac{tRNA^*}{tRNA}}{\frac{tRNA^*}{tRNA}+\tau}. \tag{S47}$$

Here, κ_{max} is the rate of tRNA transcription when all tRNA genes are fully saturated with RNA polymerase in rich growth conditions where gene dosage is high. Finally, we must establish functional forms for the tRNA dependencies on the metabolic and translation rate. Simple biochemical assumptions permit a formulation of a Michaelis-Menten function for

each rate. Noting that the translation rate γ is defined as $\gamma \equiv \frac{v_{tl}}{m_{Rb}}$, where v_{tl} is the translation speed and m_{Rb} is the proteinaceous mass of a single ribosome, we take $\gamma(tRNA^*)$ to be of the form

$$\gamma(tRNA^*) = \frac{v_{tl}^{(max)}}{m_{Rb}} \frac{tRNA^*}{tRNA^* + K_M^{(tRNA^*)}}, \tag{S48}$$

where $v_{tl}^{(max)}$ is the maximum translation speed and $K_M^{(tRNA^*)}$ is the Michaelis-Menten constant. A similar argument can be made for the dependence of the metabolic rate ν on the uncharged-tRNA concentration,

$$\nu(tRNA) = \nu_{max} \frac{tRNA}{tRNA + K_M^{(tRNA)}}, \tag{S49}$$

with $K_M^{(tRNA)}$ being another Michaelis-Menten constant. Together, Equations S42 through S49 mathematically describe a model for ppGpp-dependent regulation of translational and metabolic fluxes. We note here that the presented relations so far do not consider how the metabolic rate changes with the nutrient availability in the environment (later discussed in Sec. 11.7)

In principle, an analytical solution for this system of ODEs can be found, though it precludes evaluation by hand and is computationally intensive. While we do not solve this system of ODEs analytically here, we can numerically integrate them to sufficiently approximate the steady-state behavior. Depending on the choice of parameter values, such an approach can yield an allocation scenario nearly indistinguishable from that of the optimal allocation scenario (scenario III) of the simple model [main text Fig. 3 (E, F)] introduced in the main text.

11.2 Optimal allocation emerges from flux-parity regulation

While the previous section lays out the mathematics of the flux-parity model, we now discuss how this regulation scheme can lead to an optimal allocation. Towards this goal we first discuss in more detail what we mean when we say 'flux-parity'. As described in the main text, we define flux-parity as a balance *and* mutual maximization of (i) the flux of uncharged-tRNAs through metabolism (termed the *metabolic flux* J_{Mb}) and (ii) the flux of charged-tRNAs through protein synthesis (termed the *translational flux* J_{Tl}). To demonstrate this point, assume that we can decouple the dependence of the allocation parameter ϕ_{Rb} from the ratio of charged- to uncharged-tRNAs. Mathematically speaking, we can define the metabolic flux as the collective action of metabolic proteins,

$$J_{Mb} = \nu(tRNA)\phi_{Mb} = \frac{\nu_{max} tRNA\,(1 - \phi_O - \phi_{Rb})}{tRNA + K_M^{tRNA}}. \tag{S50}$$

Similarly, we can state that the translational flux is the collective action of ribosomal proteins,

$$J_{Tl} = \frac{\gamma_{max} tRNA^* \phi_{Rb}}{tRNA^* + K_M^{tRNA^*}} \tag{S51}$$

So long as these fluxes are equivalent, a steady-state is satisfied. However, this steady-state is not necessarily the optimal value. This is illustrated in Fig. S6. For example, if we consider that ϕ_{Rb} is too large for the given condition [Fig. S6(left)], a specific steady-state is realized (black point). If ϕ_{Rb} is further increased, the value of both the metabolic and translational fluxes (dashed lines) must decrease to reach a new steady-state and growth-rate thus declines. However, if ϕ_{Rb} is decreased, the value of both fluxes increase and growth-rate thus also increases as well. At optimum allocation [where growth is locally maximized, Fig. S6(middle)], any perturbation to ϕ_{Rb} will necessarily results in a decrease in the fluxes, indicating that at the optimal allocation the fluxes are *mutually maximized*.

As the concentrations of both tRNA species (Eqs. S42 and S43) are dependent on the allocation towards ribosomes ϕ_{Rb} in inverse ways, the ratio of their concentrations acts as an effective sensor of the magnitude of either flux. A large charged- to uncharged-tRNA ratio indicates that there is an abundance of charged-tRNAs, suggesting that the translational flux is too low. Conversely, a small charged- to uncharged-tRNA ratio indicates a translational flux that is too large, diminishing the metabolic flux. By tying the allocation towards ribosomes ϕ_{Rb} to this ratio, an allocation can emerge that optimizes the fluxes and thus growth.

11.3 Parameter dependence of the flux-parity model

In the main text, we present a solution of the flux-parity model which nearly identically matches the solution for scenario III in which optimal allocation was ensured by hand (Fig. 3 E and F). Here, we discuss the parametric sensitivity of this matching and comment on our rationale for choosing specific values.

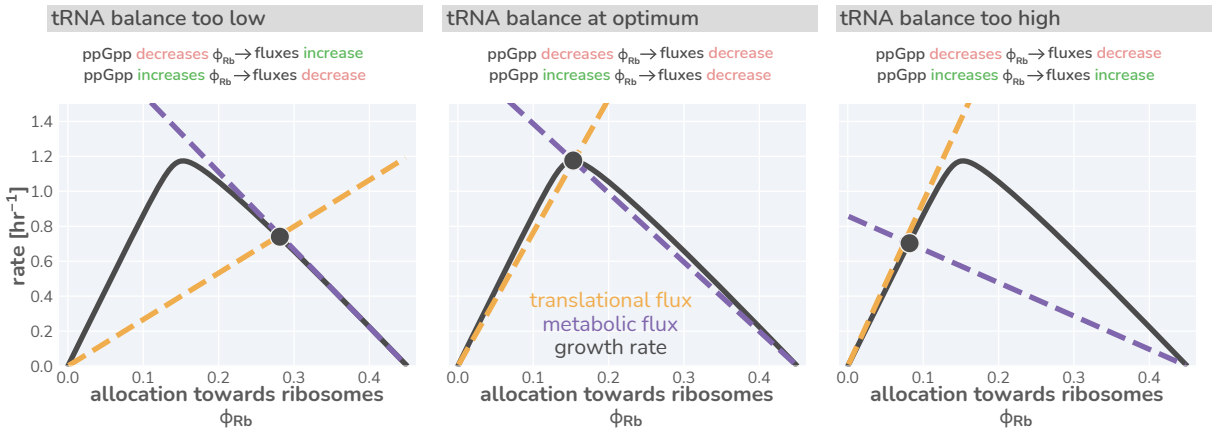

Figure S6: Flux-parity directs allocation parameters towards an optimum. Black lines represent the steady-state growth rate as a function of the allocation towards ribosomes ϕ_{Rb}. Dashed gold and purple lines correspond to the translational and metabolic fluxes, with their intersection indicating the steady-state. The different panels consider from left to right three scenarios with a too low, optimal, and too high allocation towards ribosomes. An interactive version of this figure is available on the paper website

In the previous subsections, we defined the equations of the flux-parity model (Eqs. S42 - S49). In comparison with the simplistic model where the allocation towards ribosomes is a parameter, we have introduced two Michaelis-Menten parameters (K_M^{tRNA} and $K_M^{tRNA^*}$), one ppGpp-specific sensitivity parameter (τ) and a maximal uncharged-tRNA synthesis rate (κ_{max}). While we can use *in vivo* and *in vitro* studies for estimates of these parameters, it is useful to explore how sensitive the model predictions are to precise values.

We first explore how different combinations of parameter values for the Michaelis-Menten constants impact the predictions. We chose to evaluate the steady-state conditions of the flux-parity model for pairwise combinations of a range of K_M values spanning three orders of magnitude from $\approx 10^{-5}$ (≈ 20 μM) to $\approx 10^{-2}$ (≈ 20 mM), which covers typical physiological ranges of Michaelis-Menten constants. With the steady-state solutions in hand, we the computed the absolute difference in the steady-state allocation towards ribosomes ϕ_{Rb} from that predicted by the optimal allocation (scenario III) of the simple allocation model where allocation parameters are set by hand [Fig S7(A)]. We found that the precise value of either Michaelis-Menten parameter was less important than their relative values. In fact, we found that a near identical match to the optimal allocation emerged when the parameters were of approximately equal value, $K_M^{tRNA} \approx K_M^{tRNA^*}$. This makes sense from a theoretical perspective as both metabolism and translation are feeding into each other's precursor pools. If one K_M was significantly larger than another, the sensitivity of the ppGpp system to the charged- to uncharged-tRNA ratio would also need to be significantly adjusted to accommodate the drastically different kinetics. At particularly large values ($K_M^{tRNA^*} \approx K_M^{tRNA} \approx 10^{-3}$), this one-to-one ratio breaks down with an optimal solution emerging when $K_M^{tRNA} > K_M^{tRNA^*}$. However, this difference is small and maintaining a $K_M^{tRNA} \approx K_M^{tRNA^*}$ deviates from the optimal allocation by $\leq 1\%$.

Like the Michaelis-Menten constants, there is also a strong interdependent relationship between the value of the uncharged-tRNA synthesis rate κ_{max} and the ppGpp sensitivity parameter τ, which sets the charged- to uncharged-tRNA ratio at which ϕ_{Rb} is half-maximal. We also did a wide pairwise parameter value scan over the range $\tau \in [10^{-5}, 10]$ and $\kappa_{max} \in [10^{-5}, 1]$ hr^{-1}, which spans reasonable physiological values [Fig. S7(B)]. We again see a region of parameter space where the precise values are largely unimportant, so long as the magnitude of τ is approximately three times larger than κ_{max}. At particularly low values of κ_{max} ($\leq 10^{-4}$ hr^{-1}), this dependence again breaks down with $\tau \approx 1.5$ yielding approximately optimal results.

The inverse relationship between these two parameters also makes sense from a biological perspective. There is only one way by which charged-tRNAs can be synthesized (via metabolism), but two ways in which uncharged-tRNAs can be synthesized (via translation or via transcription). Thus, if the transcription rate of uncharged-tRNAs is very large compared to the synthesis rate by translation, it becomes difficult for the charged- to uncharged-tRNA ratio to become ≥ 1. To appropriately adjust the allocation towards ribosomes ϕ_{Rb} (as in Eq. S46), τ must be at a lower value to remain responsive to changes in the charged- to uncharged-tRNA ratio.

This sensitivity analysis demonstrates a large amount of parametric degeneracy in the flux-parity allocation model. Thus, there is a large parameter space of physiologically-feasible values where flux-parity can operate to effect an optimal allocation strategy. This degeneracy suggests that an optimal allocation strategy could more easily evolve once the basic regulation strategies are in place as it does not rely on the simultaneous fine-tuning of every parameter describing the different processes. Given this degeneracy, one can also reduce the dimensionality of the model even further by asserting

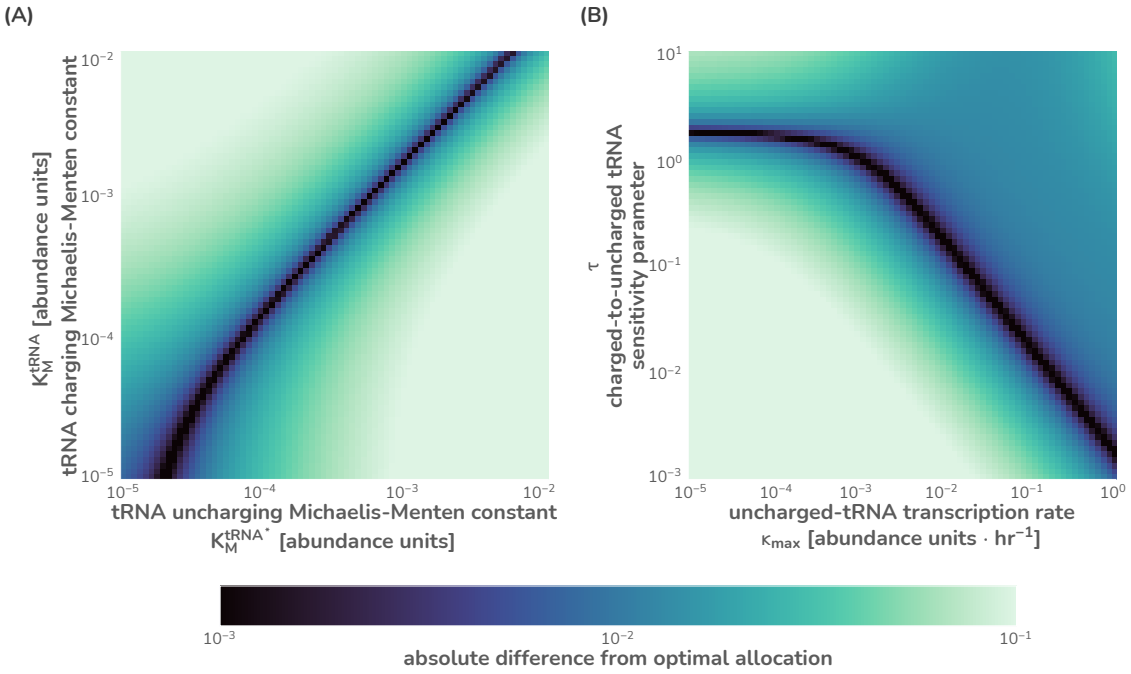

Figure S7: Sensitivity analysis of the flux-parity model for key parameters. To demonstrate the sensitivity of the flux-parity model to yield approximately identical predictions to optimal allocation, parameter values spanning several orders of magnitude were compared for the (A) Michaelis-Menten constants and (B) the tRNA synthesis rate κ and ppGpp sensitivity parameter τ. Both (A) and (B) were evaluated at a single metabolic rate $\nu_{max} = 4.5$ hr^{-1}. The absolute difference from the flux-parity determined allocation and the optimal allocation was computed and is shown on a logarithmic color scale from near-identical (purple) to significantly different (light green). All parameter values except for those being explored were kept the same as listed in Table S1

.

that the K_M's must be approximately equal,

$$K_M^* = K_M^{\text{tRNA}} \approx K_M^{tRNA^*} \tag{S52}$$

and that the magnitude of κ_{max} must be one-third that of the sensitivity parameter τ,

$$\kappa_{max} \approx \frac{\tau}{3}\frac{1}{\text{hr}}. \tag{S53}$$

While this reduces the flux-parity model to only four critical parameters (τ, K_M^*, γ_{max}, and ν_{max}), we chose to keep all parameters independent and assigned their values as described in Table S1.

11.4 Incorporating effects of ribosome-targeting antibiotics

To extend the flux-parity allocation model and incorporate the effects of antibiotic treatment, we must consider the mechanism of action of the antibiotic, specifically chloramphenicol. Chloramphenicol is a bacteriostatic antibiotic with tightly, but reversibly, binds to the ribosome. Once bound, the ribosome is unable to resume translation until chloramphenicol dissociates. Thus, we can model the effect of this drug by enumerating the probability that chloramphenicol is bound to a ribosome P_{bound} at a given concentration c_{cm}. Mathematically, this can be stated as

$$P_{\text{bound}} = \frac{c_{cm}}{c_{cm} + K_D^{cm}}, \tag{S54}$$

where K_D^{cm} is an effective dissociation constant of chloramphenicol to a unit of ribosomal mass accounting for kinetics transport and ribosome binding. We can then say that the probability of a ribosome being active is equal to the probability of a ribosome being *unbound*,

$$P_{\text{active}} = 1 - P_{\text{bound}} = 1 - \frac{c_{cm}}{c_{cm} + K_D^{cm}}. \tag{S55}$$

As only active ribosomes will contribute to the accumulation of biomass, we must rewrite the dynamics as

$$\frac{dM}{dt} = \gamma(tRNA^*)M_{Rb}^{\text{active}} = \gamma(tRNA^*)P_{\text{active}}M_{Rb}. \tag{S56}$$

To make the predictions shown in Fig. 5 (A) of the main text, we assumed that the chloramphenicol concentration in the growth medium is equal to the intracellular concentration and take $K_D^{cm} \approx 0.5$ nM.

11.5 Incorporating effects of excess protein stress

We consider that the excess protein synthesis can be modeled as the introduction of a new protein class, which we consider to have a total mass of M_X. Following the allocation parameters of the flux-parity model as defined in Eq. S44, we can introduce a new allocation parameter ϕ_X such that

$$\frac{dM_X}{dt} = \phi_X \frac{dM}{dt} \; ; \; \phi_O + \phi_{Mb} + \phi_{Rb} + \phi_X = 1. \tag{S57}$$

In the right-hand panel of Fig. 5B in the main text, we show that a collection of data can be collapsed onto a single line that relates the relative change in growth rate as a function of the excess protein that is synthesized. While we cannot fully solve the flux-parity model analytically, we can derive an analytical expression of this relation. Specifically, we note that the steady-state growth rate in the absence of excess expression λ follows the simple relation

$$\lambda = \gamma(tRNA^*)\phi_{Rb}\left(\frac{tRNA^*}{tRNA}\right) = \gamma_{max}(1-\phi_O)\frac{tRNA^*}{tRNA^* + K_M^{tRNA^*}}\frac{\frac{tRNA^*}{tRNA}}{\frac{tRNA^*}{tRNA}+\tau}. \tag{S58}$$

This can be easily extended to compute the growth rate under excess protein synthesis λ_X as

$$\lambda_x = \gamma(tRNA^*)\phi_{Rb}\left(\frac{tRNA^*}{tRNA}\right) = \gamma_{max}(1-\phi_O-\phi_X)\frac{tRNA^*}{tRNA^* + K_M^{tRNA^*}}\frac{\frac{tRNA^*}{tRNA}}{\frac{tRNA^*}{tRNA}+\tau}. \tag{S59}$$

We can take the ratio of these growth rates to yield an expression for the collapse function

$$\frac{\lambda_X}{\lambda} = \frac{\gamma_{max}(1-\phi_O-\phi_X)\frac{tRNA^*}{tRNA^*+K_M^{tRNA^*}}\frac{\frac{tRNA^*}{tRNA}}{\frac{tRNA^*}{tRNA}+\tau}}{\gamma_{max}(1-\phi_O)\frac{tRNA^*}{tRNA^*+K_M^{tRNA^*}}\frac{\frac{tRNA^*}{tRNA}}{\frac{tRNA^*}{tRNA}+\tau}}. \tag{S60}$$

If we assume that the excess protein synthesis affects *only* ϕ_X, leaving all other parameters untouched, Eq. S60 reduces to the concise form

$$\frac{\lambda_X}{\lambda} = \frac{1-\phi_O-\phi_X}{1-\phi_O}, \tag{S61}$$

which is the linear relation plotted in the right-hand side of Fig. 5B of the main text.

Aside from the collapse, we also show how the flux-parity model quantitatively predicts the growth rate as a function of excess protein for three different media (Fig. 5C, center panel). In this case, we require some knowledge of what the metabolic rate ν_{max} is for those specific conditions. As the metabolic rate is an efficient rate incorporating the action of different metabolic reactions and serving as a proxy of the nutrient quality, it is not possible to make an *a priori* estimate of its value. To nevertheless estimate ν_{max} for each condition, we determined its value by using the simple allocation model as encoded in Sec. 6, assuming the growth rate λ and the ribosomal content describes the allocation towards ribosomes ϕ_{Rb}. Under the simple allocation model, we note that an expression for the metabolic rate can be solved from the steady-state precursor concentration c_{pc}^* (Eq. S19) to yield

$$\nu_{max} = \frac{\lambda\left(c_{pc}+1\right)}{1-\phi_O-\phi_{Rb}}. \tag{S62}$$

The steady-state precursor concentration c_{pc}^* can be solved from the definition of the steady-state growth rate and has the form

$$c_{pc}^* = \frac{K_D^{c_{pc}}\lambda}{\phi_{Rb}\gamma_{max}\left(1-\frac{\lambda}{\phi_{Rb}}\right)}. \tag{S63}$$

Combining Eqs. S62 and S63 yields an expression for the maximal metabolic rate ν_{max},

$$\nu_{max} = \frac{\lambda}{1-\phi_O-\phi_{Rb}}\left(\frac{K_D^{c_{pc}}\lambda}{\phi_{Rb}\gamma_{max}\left(1-\frac{\lambda}{\phi_{Rb}}\right)}+1\right). \tag{S64}$$

Thus, given knowledge of the steady-state growth rate λ and the allocation towards ribosomes ϕRb (which are both measured quantities), the value of ν_{max} can be derived.

11.6 Incorporating effects of nutrient upshifts

To model the dynamics of growth in fluctuating conditions, we asserted that a nutritional upshift is equivalent to an instantaneous change in the metabolic rate such that $\nu_{max}^{preshift} < \nu_{max}^{postshift}$. However, this is not completely sufficient to capture the phenomenology that is observed. It is becoming exceedingly clear that bacterial cells are non-optimal in *what* genes they express, with many proteins that are synthesized are ultimately useless in the specific condition [47]. This can have very important effects on the growth rate as any amount of conditionally useless protein that's synthesized consumes resources that could otherwise be partitioned to the proteins that need to be synthesized. To incorporate this effect, we introduce another protein class with an allocation parameter $\phi_{\emptyset}$. As the degree of conditionally useless expression is significantly more pronounced in slow rather than fast conditions [22, 37, 47], we further asserted that the magnitude of this sector also changed in response to the nutritional upshift such that $\phi_{\emptyset}^{preshift} > \phi_{\emptyset}^{postshift}$. The precise value of this sector is less important than the difference in the pre- and post-shift condition and can be considered as an additional rescaling factor as described in Sec. 8. Thus, for all nutritional shifts in this work, we considered that $\phi_{\emptyset}^{postshift} = 0$ and the value of $\phi_{\emptyset}^{preshift}$ to be linearly proportional to the difference in the growth rates between the pre- and post-shift conditions.

11.7 Incorporating effects of nutrient depletion

Up to this point, we have explored the flux-parity model under the assumption that the nutrients in the environment were saturating, such that $\nu(c_{nt}) \approx \nu_{max}$. However, a dependence on the environmental nutrient concentration c_{nt} can be easily included in the definition of the metabolic rate ν as

$$\nu(tRNA, c_{nt}) = \nu_{max}\left(\frac{tRNA}{tRNA + K_M^{tRNA}}\right)\left(\frac{c_{nt}}{c_{nt}+K_M^{c_{nt}}}\right), \tag{S65}$$

where $K_M^{c_{nt}}$ is the Michaelis-Menten constant (described in Sec. 6). We can then model the dynamics of the nutrient concentration c_{nt} in a batch-culture system as

$$\frac{dc_{nt}}{dt} = -\frac{\nu(tRNA, c_{nt})M_{Mb}}{Y}, \tag{S66}$$

where Y is the yield coefficient.

12 Data Sets

This work leverages a large collection of data, primarily from *E. coli*, to evaluate the accuracy of our model in describing biological phenomena. These data come from a range of studies spanning around 50 years of measurements from different groups and different geographical locations. Collecting and curating this large data set required the manual transcribing of data from papers as well as various standardization steps to ensure that measurements were truly comparable between studies, as is outlined in Table S2.

13 Supplementary Tables

Parameter	Value [Units]	Reference	Notes
Maximum translation speed $v_{tl,max}$	≈ 20 [AA $\cdot$ s^{-1}]	Refs. [19, 48]	Taken maximum values as typically reported in literature and textbooks
Proteinaceous mass of ribosome m_{Rb}	7459 [AA]	BNID:101175 (Ref. [23])	–
Maximum translation rate γ_{max}	≈ 9.65 [hr^{-1}]	This study	Calculated as $\gamma_{max} = v_{tl,max}/m_{Rb}$
Maximum metabolic rate ν_{max}	$0.001 - 20$ [hr^{-1}]	This study	Defined as wide range to cover physiological growth rates
Precursor dissociation constant $K_M^{c_{pc}}$	$\approx$ 0.03 [abundance] ($\approx$ 80 [mM])	This study (Ref. [49])	Approximately equivalent to total free amino acid pool concentration.
Nutrient dissociation constant $K_M^{c_{nt}}$	≈ 0.5 [mM]	Ref. [50]	Monod constant for *E. coli* growth on glucose
'Other' protein allocation parameter ϕ_O	≈ 0.55	Ref. [42]	–
Charged-tRNA effective dissociation constant $K_M^{(tRNA^*)}$	$\approx 3 \times 10^{-5}$ [abundance] ($\approx$ 80 μM)	This study	Estimated order of magnitude. See Section 11.3 for discussion of value dependence
Uncharged-tRNA effective dissociation constant $K_M^{(tRNA)}$	$\approx 3 \times 10^{-5}$ [abundance] ($\approx$ 80 μM)	This study	Estimated order of magnitude. See Section 11.3 for discussion of value dependence
Charged-to-uncharged-tRNA ratio threshold parameter τ	≈ 1	This study	Estimated value. See section 11.3 for deeper discussion
Uncharged-tRNA maximum synthesis rate κ_{max}	≈ 0.001 [abundance $\cdot$ hr^{-1}] ($\approx$ 300 tRNA$\cdot$s^{-1}	This study	Estimated value. See footnote *a*.

Table S1: Reference parameter set for *E. coli* used in this work.

a: Value was estimated as follows. The maximum tRNA synthesis rate was taken to be that in very rich media. In these conditions, each *E. coli* cell has $\approx$ 5 - 8 copies of its genome and each genome is assumed to have $\approx$ 64 copies of tRNA genes. At a transcription rate of 40 nt/s, each tRNA gene can produce $\approx$ 1 tRNA per second [22]. Together, this yields an estimate for the maximum rate of tRNA synthesis to be $\kappa_{max} \approx 5\,\text{genomes} \times 64\,\text{genes/genome} \times 1\,\text{tRNA/gene/sec} \approx 320\,\text{tRNA/sec}$. Assuming each tRNA can be charged with an amino acid (and thus has a mass of 1 AA) and that in the fastest growth conditions there are $\approx 10^9$ AA / cell [22], one arrives at an abundance synthesis rate of $\kappa_{max} \approx 0.001$ hr[$^{-1}$].

Study	Experiment	Source
Albertson & Nyström, 1994 [51]	Translation speed	Reported in text, paragraph 1 on pg. 185
Basan *et al.*, 2015 [52]	Ribosome content	RNA/Protein[a] in Table S4
	LacZ overexpression	Digitized[b] from Fig. S4B
Bentley *et al.*, 1990 [53]	β-lactamase overexpression	Digitized[b] from Fig. 10
Bremer & Dennis, 2008 [19]	Ribosome content	RNA/Protein [a] Table 2
	Translation speed	Recalculated[c] from Table 2
Bren *et al.*, 2013 [54]	Starvation response	Digitized[b] from Fig. S3
Brunschede *et al.*, 1977 [55]	Ribosome content	RNA/Protein[a] in Table 1
	Nutrient upshift[d]	Measurement of growth rate in Table 2
Coffman *et al.*, 1971 [56]	Translation speed	Taken from Table 1 in Ref. [57]
Dai *et al.*, 2016 [28]	Ribosome content	RNA/Protein[a] in Table S3
	Ribosome content under chloramphenicol	RNA/Protein[a] in Table S5
	Translation speed	Elongation rate in Table S1
	Translation speed under chloramphenicol	Elongation rate in Table S4
Dalbow & Young, 1975 [58]	Translation speed	Table 2
Dennis & Bremer, 1974 [59]	Translation speed	Reported in text, paragraph 1 on pg. 418.
Erickson *et al.*, 2017 [60]	Ribosome content	Digitized[b] from RNA/Protein[a] in Fig. S1
	Nutrient upshift	Digitized[b] from Fig. 1 & Fig. S3.
Dong *et al.*, 1995 [61]	EF-Tu & LacZ overexpression	Digitized[b] from Fig. 4 in Ref. [11]
Forchhammer & Lindahl, 1971 [48]	Ribosome content	RNA/Protein[a] in Table 1
	Translation speed	Recalculated[c] from Table 1
Gausing, 1972 [62]	Translation speed	Reported in text, paragraph 4 of pg. 539.
Hernandez & Bremer, 1993 [6]	Translation speed	Calculated from RNA/Protein in Table 2
Kepes & Beguin, 1966 [63]	Translation speed	Taken from Table 1 in Ref. [57]
Korem Kohanim *et al.*, 2018 [33]	Nutrient upshift	Table S1
Lacroute & Stent, 1968 [64]	Translation speed	Taken from Table 1 in Ref. [57]
Li *et al.*, 2014	Ribosome content	Ribosome profiling[e]
Li *et al.*, 2018	Ribosome content	RNA/Protein[a] in Table S2
	Nutrient upshift[d]	Digitized[b] from Fig. 4
Mori *et al.*, 2017 [32]	Ribosome content	Digitized[b] from RNA/Protein[a] in Fig. S2
	Nutrient upshift[d]	Digitized[b] from Fig. S4
Morris & Hansen, 1973 [65]	Translation speed	Taken from Table 1 in Ref. [57]
Oldewurtel *et al.*, 2021 [17]	Nutrient upshift[d]	Digitized[b] from Fig. 3A
Panlilio *et al.*, 2021 [66],	Nutrient upshift[d]	Digitized[b] from Fig. 2A and S11A
Pederson, 1984 [67]	Translation speed	Taken from parenthetical values Table 1.
Schmidt *et al.*, 2016 [37]	Ribosome content	Mass spectrometry[e]
Schleif, 1967 [68]	Translation speed	Reported in text, middle of pg. 53
	Nutrient upshift[d]	Digitized[b] from Fig. 9
Schleif *et al.*, 1973 [69]	Translation speed	Taken from Table 1 in Ref. [57]
Scott *et al.*, 2010 [11]	Ribosome content	RNA/Protein[a] in Table S1
	LacZ overexpression	Digitized[b] from Fig. 4
Si *et al.*, 2017 [70]	Ribosome content	RNA/Protein[a] in Supplementary Data
Sloan & Urban, 1976 [71]	Nutrient upshift[d]	Taken from Table S2 of Ref. [33]
Wu *et al.*, 2021 [14]	Ribosome content	Digitized[b] from RNA/Protein[a] in Fig. 3
	Translation speed	Digitized[b] from Fig. 3E
You *et al.*, 2013 [72]	Ribosome content	RNA/Protein[a] from Table S10
Young & Bremer, 1976 [57]	Translation speed	Table 1
Zhu & Dai, 2019 [73]	Ribosome content	Digitized[b] from RNA/Protein[a] in Fig. 2D

Table S2: *E. coli* data used in this work and the corresponding sources.
a: Converted to ribosome content by assuming 0.86 μg of rRNA per 1 μg RNA and 0.53 μg of ribosomal protein per 1 μg of rRNA. This yields a conversion factor of $\frac{M_{Rb}}{M} = 0.4558 \times \frac{RNA}{Protein}$. b: Source data was not available, so data was determined from figures using WebPlotDigitizer [74]. c: Original values were calculated assuming $\approx$ 70% of ribosomes were active. We assume all ribosomes are active and recalculated the values accordingly. d: Growth rate immediately following the shift $\lambda_i^\dagger$ was calculated by averaging values within first 20 min. after the shift to be consistent with procedure reported by Korem Kohanim *et al.*, 2018 [33]. e: Original data curated and standardized by Belliveau & Chure *et al.*, 2021 [22].

Parameter	Value [Units]	Reference	Notes
Maximum translation speed $v_{tl,max}$	≈ 10 [AA $\cdot$ s^{-1}]	BNID: 107871 Ref. [23]	Taken as maximum value typically reported in text books
Proteinaceous mass of ribosome m_{Rb}	11984 [AA]	Ref. [75]	-
Maximum translation rate γ_{max}	≈ 3.00 [hr^{-1}]	This study	Calculated as $\gamma_{max} = v_{tl,max}/m_{Rb}$
Maximum metabolic rate ν_{max}	0.001 - 20 [hr^{-1}]	Defined as a wide range to cover physiological growth rates	
Precursor Michaelis-Menten constant $K_M^{c_{pc}}$	$\approx$ 0.01 [abundance] ($\approx$ 30 mM)	Ref. [76]	Corresponds to standing concentration of free amino acids at moderate growth rate.

Table S3: Reference parameter set for *S. cerevisiae* used in this work.

Study	Experiment	Source
Bonven & Gulløv, 1979 [77]	Translation speed	Taken from Table 1
Lacroute, 1973 [78]	Translation speed	Recalculated[a] from pg. 325
Metzl-Raz *et al.*, 2017 [31]	Ribosome content	Digitized[a] from Fig. 2A
Paulo *et al.*, 2015 [79]	Ribosome content	Digitized[b] from Fig. 2A in Ref. [31]
Paulo *et al.*, 2016 [80]	Ribosome content	Digitized [b] from Fig. 2A in Ref. [31]
Riba *et al.*, 2019 [81]	Translation speed	Taken from caption in Fig. 3B
Siwiak & Zielenkiewcz, 2010 [82]	Translation speed	taken from Table 1
Waldron & Lacroute, 1975 [83]	Ribosome content	Calculated[c] from Tables 4 and 5
Xia *et al.*, 2021 [84]	Ribosome content	Digitized[b] from Fig. 1C

Table S4: *S. cerevisiae* data used in this work and the relevant sources.
a: Original values were calculated assuming $\approx$ 70% of ribosomes were active. We assume all ribosomes are active and recalculated the values accordingly.
b: Source data was not available, so data was approximated from Figure using WebPlotDigitizer [74].
c: Calculated given the total mass of protein per cell in Table 5 and the number of Ribosomes in Table 4. A length of 11,984 AA per ribosome and an average amino acid mass of 110 Da / AA was used to calculate total ribosomal mass.

References

[1] P Verhulst. Recherches mathématiques sur la loi d'accroissement de la population. *Nouv. mém. de l'Academie Royale des Sci. et Belles-Lettres de Bruxelles*, 18, 1845.

[2] Jacques Monod. *Recherches sur la croissance des cultures bacteriennes,*. Hermann & cie, Paris, 1942. OCLC: 6126763.

[3] Jonathan R. Karr, Jayodita C. Sanghvi, Derek N. Macklin, Miriam V. Gutschow, Jared M. Jacobs, Benjamin Bolival, Nacyra Assad-Garcia, John I. Glass, and Markus W. Covert. A Whole-Cell Computational Model Predicts Phenotype from Genotype. *Cell*, 150(2):389–401, July 2012.

[4] Xiao-Pan Hu, Hugo Dourado, Peter Schubert, and Martin J. Lercher. The protein translation machinery is expressed for maximal efficiency in *Escherichia* coli. *Nature Communications*, 11(1):5260, October 2020.

[5] Derek N. Macklin, Travis A. Ahn-Horst, Heejo Choi, Nicholas A. Ruggero, Javier Carrera, John C. Mason, Gwanggyu Sun, Eran Agmon, Mialy M. DeFelice, Inbal Maayan, Keara Lane, Ryan K. Spangler, Taryn E. Gillies, Morgan L. Paull, Sajia Akhter, Samuel R. Bray, Daniel S. Weaver, Ingrid M. Keseler, Peter D. Karp, Jerry H. Morrison, and Markus W. Covert. Simultaneous cross-evaluation of heterogeneous *e. coli* datasets via mechanistic simulation. *Science*, 369(6502), July 2020.

[6] V.J. Hernandez and H. Bremer. Characterization of RNA and DNA synthesis in *escherichia* coli strains devoid of ppGpp. *Journal of Biological Chemistry*, 268(15):10851–10862, May 1993.

[7] Arthur L. Koch. Why can't a cell grow infinitely fast? *Canadian Journal of Microbiology*, 34(4):421–426, April 1988. Publisher: NRC Research Press.

[8] B. Magasanik, Adele K. Magasanik, and F. C. Neidhardt. Regulation of Growth and Composition of the Bacterial Cell. In *Ciba Foundation Symposium — Regulation of Cell Metabolism*, pages 334–352. John Wiley & Sons, Ltd, 1959. _eprint: https://onlinelibrary.wiley.com/doi/pdf/10.1002/9780470719145.ch16.

[9] Douwe Molenaar, Rogier van Berlo, Dick de Ridder, and Bas Teusink. Shifts in growth strategies reflect tradeoffs in cellular economics. *Molecular Systems Biology*, 5(1):323, January 2009.

[10] M. Scott, S. Klumpp, E. M. Mateescu, and T. Hwa. Emergence of robust growth laws from optimal regulation of ribosome synthesis. *Molecular Systems Biology*, 10(8):747–747, August 2014.

[11] Matthew Scott, Carl W. Gunderson, Eduard M. Mateescu, Zhongge Zhang, and Terence Hwa. Interdependence of Cell Growth and Gene Expression: Origins and Consequences. *Science*, 330(6007):1099–1102, November 2010.

[12] Nils Giordano, Francis Mairet, Jean-Luc Gouzé, Johannes Geiselmann, and Hidde de Jong. Dynamical Allocation of Cellular Resources as an Optimal Control Problem: Novel Insights into Microbial Growth Strategies. *PLOS Computational Biology*, 12(3):e1004802, March 2016.

[13] Evert Bosdriesz, Douwe Molenaar, Bas Teusink, and Frank J. Bruggeman. How fast-growing bacteria robustly tune their ribosome concentration to approximate growth-rate maximization. *The FEBS journal*, 282(10):2029–2044, May 2015.

[14] Chenhao Wu, Rohan Balakrishnan, Matteo Mori, Gabriel Manzanarez, Zhongge Zhang, and Terence Hwa. Cellular perception of growth rate and the mechanistic origin of bacterial growth laws. Preprint, Systems Biology, October 2021.

[15] Jonas van den Berg, Arnold J. Boersma, and Bert Poolman. Microorganisms maintain crowding homeostasis. *Nature Reviews Microbiology*, 15(5):309–318, May 2017. Bandiera_abtest: a Cg_type: Nature Research Journals Number: 5 Primary_atype: Reviews Publisher: Nature Publishing Group Subject_term: Cell growth;Cellular microbiology Subject_term_id: cell-growth;cellular-microbiology.

[16] M. Delarue, G. P. Brittingham, S. Pfeffer, I. V. Surovtsev, S. Pinglay, K. J. Kennedy, M. Schaffer, J. I. Gutierrez, D. Sang, G. Poterewicz, J. K. Chung, J. M. Plitzko, J. T. Groves, C. Jacobs-Wagner, B. D. Engel, and L. J. Holt. mTORC1 Controls Phase Separation and the Biophysical Properties of the Cytoplasm by Tuning Crowding. *Cell*, 174(2):338–349.e20, July 2018. Publisher: Elsevier.

[17] Enno R. Oldewurtel, Yuki Kitahara, and Sven van Teeffelen. Robust surface-to-mass coupling and turgor-dependent cell width determine bacterial dry-mass density. *Proceedings of the National Academy of Sciences*, 118(32), August 2021. Publisher: National Academy of Sciences Section: Physical Sciences.

[18] William T. Gray, Sander K. Govers, Yingjie Xiang, Bradley R. Parry, Manuel Campos, Sangjin Kim, and Christine Jacobs-Wagner. Nucleoid Size Scaling and Intracellular Organization of Translation across Bacteria. *Cell*, 177(6):1632–1648.e20, May 2019. tex.ids: gray2019a.

[19] Patrick P. Dennis and Hans Bremer. Modulation of Chemical Composition and Other Parameters of the Cell at Different Exponential Growth Rates. *EcoSal Plus*, 3(1), September 2008.

[20] Ron Milo. What is the total number of protein molecules per cell volume? A call to rethink some published values. *BioEssays*, 35(12):1050–1055, 2013. _eprint: https://onlinelibrary.wiley.com/doi/pdf/10.1002/bies.201300066.

[21] Shlomi Reuveni, Måns Ehrenberg, and Johan Paulsson. Ribosomes are optimized for autocatalytic production. *Nature*, 547(7663):293–297, July 2017.

[22] Nathan M. Belliveau, Griffin Chure, Christina L. Hueschen, Hernan G. Garcia, Jane Kondev, Daniel S. Fisher, Julie A. Theriot, and Rob Phillips. Fundamental limits on the rate of bacterial growth and their influence on proteomic composition. *Cell Systems*, July 2021.

[23] Ron Milo, Paul Jorgensen, Uri Moran, Griffin Weber, and Michael Springer. BioNumbers—the database of key numbers in molecular and cell biology. *Nucleic Acids Research*, 38(suppl_1):D750–D753, January 2010.

[24] Benjamin D. Towbin, Yael Korem, Anat Bren, Shany Doron, Rotem Sorek, and Uri Alon. Optimality and sub-optimality in a bacterial growth law. *Nature Communications*, 8(1):14123, April 2017.

[25] Martin J. Pine. Regulation of Intracellular Proteolysis in Escherichia coli. *Journal of Bacteriology*, 115(1):107–116, July 1973.

[26] Ludovico Calabrese, Jacopo Grilli, Matteo Osella, Christopher P. Kempes, Marco Cosentino Lagomarsino, and Luca Ciandrini. Role of protein degradation in growth laws. Technical report, August 2021. Company: Cold Spring Harbor Laboratory Distributor: Cold Spring Harbor Laboratory Label: Cold Spring Harbor Laboratory Section: New Results Type: article.

[27] Daniel Madar, Erez Dekel, Anat Bren, Anat Zimmer, Ziv Porat, and Uri Alon. Promoter activity dynamics in the lag phase of Escherichia coli. *BMC Systems Biology*, 7(1):136, December 2013.

[28] Xiongfeng Dai, Manlu Zhu, Mya Warren, Rohan Balakrishnan, Vadim Patsalo, Hiroyuki Okano, James R. Williamson, Kurt Fredrick, Yi-Ping Wang, and Terence Hwa. Reduction of translating ribosomes enables *Escherichia* coli to maintain elongation rates during slow growth. *Nature Microbiology*, 2(2):1–9, December 2016.

[29] Sophia Hsin-Jung Li, Zhiyuan Li, Junyoung O. Park, Christopher G. King, Joshua D. Rabinowitz, Ned S. Wingreen, and Zemer Gitai. *Escherichia coli* translation strategies differ across carbon, nitrogen and phosphorus limitation conditions. *Nature Microbiology*, 3(8), August 2018.

[30] Albert L. Müller, Wenyu Gu, Vadim Patsalo, Jörg S. Deutzmann, James R. Williamson, and Alfred M. Spormann. An alternative resource allocation strategy in the chemolithoautotrophic archaeon *Methanococcus maripaludis*. *Proceedings of the National Academy of Sciences*, 118(16), April 2021.

[31] Eyal Metzl-Raz, Moshe Kafri, Gilad Yaakov, Ilya Soifer, Yonat Gurvich, and Naama Barkai. Principles of cellular resource allocation revealed by condition-dependent proteome profiling. *eLife*, 6:e28034, August 2017.

[32] Matteo Mori, Severin Schink, David W. Erickson, Ulrich Gerland, and Terence Hwa. Quantifying the benefit of a proteome reserve in fluctuating environments. *Nature Communications*, 8(1), October 2017.

[33] Yael Korem Kohanim, Dikla Levi, Ghil Jona, Benjamin D. Towbin, Anat Bren, and Uri Alon. A Bacterial Growth Law out of Steady State. *Cell Reports*, 23(10):2891–2900, June 2018.

[34] Thomas Prossliner, Kristoffer Skovbo Winther, Michael Askvad Sørensen, and Kenn Gerdes. Ribosome Hibernation. *Annual Review of Genetics*, 52(1):321–348, November 2018.

[35] Kaspar Valgepea, Kaarel Adamberg, Andrus Seiman, and Raivo Vilu. *Escherichia coli* achieves faster growth by increasing catalytic and translation rates of proteins. *Molecular BioSystems*, 9(9):2344–2358, July 2013.

[36] Matteo Mori, Zhongge Zhang, Amir Banaei-Esfahani, Jean-Benoît Lalanne, Hiroyuki Okano, Ben C Collins, Alexander Schmidt, Olga T Schubert, Deok-Sun Lee, Gene-Wei Li, Ruedi Aebersold, Terence Hwa, and Christina Ludwig. From coarse to fine: The absolute *Escherichia coli* proteome under diverse growth conditions. *Molecular Systems Biology*, 17(5), May 2021.

[37] Alexander Schmidt, Karl Kochanowski, Silke Vedelaar, Erik Ahrné, Benjamin Volkmer, Luciano Callipo, Kèvin Knoops, Manuel Bauer, Ruedi Aebersold, and Matthias Heinemann. The quantitative and condition-dependent *Escherichia coli* proteome. *Nature Biotechnology*, 34(1):104–110, January 2016.

[38] Karl Peebo, Kaspar Valgepea, Andres Maser, Ranno Nahku, Kaarel Adamberg, and Raivo Vilu. Proteome reallocation in *Escherichia coli* with increasing specific growth rate. *Molecular BioSystems*, 11(4):1184–1193, 2015.

[39] Gene-Wei Li, David Burkhardt, Carol Gross, and Jonathan S. Weissman. Quantifying absolute protein synthesis rates reveals principles underlying allocation of cellular resources. *Cell*, 157(3):624–635, April 2014.

[40] Peter D. Karp, Suzanne M. Paley, Peter E. Midford, Markus Krummenacker, Richard Billington, Anamika Kothari, Wai Kit Ong, Pallavi Subhraveti, Ingrid M. Keseler, and Ron Caspi. Pathway Tools version 23.0: Integrated Software for Pathway/Genome Informatics and Systems Biology. *arXiv:1510.03964 [q-bio]*, November 2019. arXiv: 1510.03964.

[41] Michael Y. Galperin, Yuri I. Wolf, Kira S. Makarova, Roberto Vera Alvarez, David Landsman, and Eugene V. Koonin. COG database update: focus on microbial diversity, model organisms, and widespread pathogens. *Nucleic Acids Research*, 49(D1):D274–D281, January 2021.

[42] Sheng Hui, Josh M. Silverman, Stephen S. Chen, David W. Erickson, Markus Basan, Jilong Wang, Terence Hwa, and James R. Williamson. Quantitative proteomic analysis reveals a simple strategy of global resource allocation in bacteria. *Molecular Systems Biology*, 11(2), February 2015.

[43] Lisa U. Magnusson, Anne Farewell, and Thomas Nyström. ppGpp: a global regulator in *Escherichia coli*. *Trends in Microbiology*, 13(5):236–242, May 2005.

[44] Brent W. Anderson, Danny K. Fung, and Jue D. Wang. Regulatory Themes and Variations by the Stress-Signaling Nucleotide Alarmones (p)ppGpp in Bacteria. *Annual Review of Genetics*, 55(1), 2021. _eprint: https://doi.org/10.1146/annurev-genet-021821-025827.

[45] Anjana Srivatsan and Jue D Wang. Control of bacterial transcription, translation and replication by (p)ppGpp. *Current Opinion in Microbiology*, 11(2):100–105, April 2008.

[46] Sue Jinks-Robertson, Richard L. Gourse, and Masayasu Nomura. Expression of rRNA and tRNA genes in *escherichia* coli: Evidence for feedback regulation by products of rRNA operons. *Cell*, 33(3):865–876, July 1983.

[47] Rohan Balakrishnan, Roshali T de Silva, Terence Hwa, and Jonas Cremer. Suboptimal resource allocation in changing environments constrains response and growth in bacteria. *Molecular Systems Biology*, 17(12):e10597, December 2021. Publisher: John Wiley & Sons, Ltd.

[48] Jes Forchhammer and Lasse Lindahl. Growth rate of polypeptide chains as a function of the cell growth rate in a mutant of *Escherichia* coli. *Journal of Molecular Biology*, 55(3):563–568, February 1971.

[49] A. J. Roe, D. McLaggan, I. Davidson, C. O'Byrne, and I. R. Booth. Perturbation of anion balance during inhibition of growth of *escherichia* coli by weak acids. *Journal of Bacteriology*, 180(4):767–772, February 1998.

[50] H. Senn, U. Lendenmann, M. Snozzi, G. Hamer, and T. Egli. The growth of *escherichia* coli in glucose-limited chemostat cultures: a re-examination of the kinetics. *Biochimica Et Biophysica Acta*, 1201(3):424–436, December 1994.

[51] Nan H. Albertson and Thomas Nyström. Effects of starvation for exogenous carbon on functional mRNA stability and rate of peptide chain elongation in *escherichia* coli. *FEMS Microbiology Letters*, 117(2):181–187, April 1994.

[52] Markus Basan, Manlu Zhu, Xiongfeng Dai, Mya Warren, Daniel Sévin, Yi-Ping Wang, and Terence Hwa. Inflating bacterial cells by increased protein synthesis. *Molecular Systems Biology*, 11(10):836, October 2015.

[53] W. E. Bentley, N. Mirjalili, D. C. Andersen, R. H. Davis, and D. S. Kompala. Plasmid-encoded protein: the principal factor in the "metabolic burden" associated with recombinant bacteria. *Biotechnology and Bioengineering*, 35(7):668–681, March 1990.

[54] Anat Bren, Yuval Hart, Erez Dekel, Daniel Koster, and Uri Alon. The last generation of bacterial growth in limiting nutrient. *BMC Systems Biology*, 7(1):27, March 2013.

[55] H Brunschede, T L Dove, and H Bremer. Establishment of Exponential Growth After a Nutritional Shift-Up in *Escherichia coli* B/r: Accumulation of Deoxyribonucleic Acid, Ribonucleic Acid, and Protein. *Journal of Bacteriology*, 129:14, 1977.

[56] Robert L. Coffman, Thomas E. Norris, and Arthur L. Koch. Chain elongation rate of messenger and polypeptides in slowly growing *escherichia* coli. *Journal of Molecular Biology*, 60(1):1–11, August 1971.

[57] R. Young and H. Bremer. Polypeptide-chain-elongation rate in *escherichia* coli B/r as a function of growth rate. *The Biochemical Journal*, 160(2):185–194, November 1976.

[58] D G Dalbow and R Young. Synthesis time of -galactosidase in *escherichia* coli B/r as a function of growth rate. *Biochemical Journal*, 150(1):13–20, July 1975.

[59] Patrick P. Dennis and Hans Bremer. Differential rate of ribosomal protein synthesis in *escherichia* coli B/r. *Journal of Molecular Biology*, 84(3):407–422, April 1974.

[60] David W. Erickson, Severin J. Schink, Vadim Patsalo, James R. Williamson, Ulrich Gerland, and Terence Hwa. A global resource allocation strategy governs growth transition kinetics of *Escherichia coli*. *Nature*, 551(7678):119–123, November 2017.

[61] H Dong, L Nilsson, and C G Kurland. Gratuitous overexpression of genes in *escherichia* coli leads to growth inhibition and ribosome destruction. *Journal of Bacteriology*, 177(6):1497–1504, March 1995. Publisher: American Society for Microbiology.

[62] Kirsten Gausing. Efficiency of protein and messenger RNA synthesis in bacteriophage T4-infected cells of *escherichia* coli. *Journal of Molecular Biology*, 71(3):529–545, November 1972.

[63] Adam Kepes and Simone Beguin. Peptide chain initiation and growth in the induced synthesis of -galactosidase. *Biochimica et Biophysica Acta (BBA) - Nucleic Acids and Protein Synthesis*, 123(3):546–560, September 1966.

[64] F. Lacroute and G. S. Stent. Peptide chain growth of -galactosidase in *escherichia* coli. *Journal of Molecular Biology*, 35(1):165–171, July 1968.

[65] David R. Morris and Mogens T. Hansen. Influence of Polyamine Limitation on the Chain Growth Rates of -Galactosidase and of Its Messenger Ribonucleic Acid. *Journal of Bacteriology*, 116(2):588–592, November 1973.

[66] Mia Panlilio, Jacopo Grilli, Giorgio Tallarico, Ilaria Iuliani, Bianca Sclavi, Pietro Cicuta, and Marco Cosentino Lagomarsino. Threshold accumulation of a constitutive protein explains *E. coli* cell division behavior in nutrient upshifts. preprint, Cell Biology, August 2020.

[67] S Pedersen. *Escherichia coli* ribosomes translate in vivo with variable rate. *The EMBO Journal*, 3(12):2895–2898, December 1984.

[68] Robert Schleif. Control of Production of Ribosomal Protein. *Journal of Molecular Biology*, 27:15, 1967.

[69] Robert Schleif, Winand Hess, Solomon Finkelstein, and D. Ellis. Induction Kinetics of the l-Arabinose Operon of *Escherichia coli*. *Journal of Bacteriology*, 115(1):9–14, July 1973.

[70] Fangwei Si, Dongyang Li, Sarah E. Cox, John T. Sauls, Omid Azizi, Cindy Sou, Amy B. Schwartz, Michael J. Erickstad, Yonggun Jun, Xintian Li, and Suckjoon Jun. Invariance of Initiation Mass and Predictability of Cell Size in *Escherichia* coli. *Current Biology*, 27(9):1278–1287, May 2017.

[71] J B Sloan and J E Urban. Growth response of *escherichia* coli to nutritional shift-up: immediate division stimulation in slow-growing cells. *Journal of Bacteriology*, 128(1):302–308, October 1976.

[72] Conghui You, Hiroyuki Okano, Sheng Hui, Zhongge Zhang, Minsu Kim, Carl W. Gunderson, Yi-Ping Wang, Peter Lenz, Dalai Yan, and Terence Hwa. Coordination of bacterial proteome with metabolism by cyclic AMP signalling. *Nature*, 500(7462), August 2013.

[73] Manlu Zhu and Xiongfeng Dai. Growth suppression by altered (p)ppGpp levels results from non-optimal resource allocation in Escherichia coli. *Nucleic Acids Research*, 47(9):4684–4693, May 2019.

[74] Ankit Rohatgi. Webplotdigitizer: Version 4.5, 2021.

[75] Adriana Verschoor, Jonathan R. Warner, Suman Srivastava, Robert A. Grassucci, and Joachim Frank. Three-dimensional structure of the yeast ribosome. *Nucleic Acids Research*, 26(2):655–661, January 1998.

[76] T. G Watson. Amino-acid Pool Composition of *Saccharomyces cerevisiae* as a Function of Growth Rate and Amino-acid Nitrogen Source. *Journal of General Microbiology*, 96(2):263–268, 1976.

[77] Bjarne Bonven and Kay Gulløv. Peptide chain elongation rate and ribosomal activity in Saccharomyces cerevisiae as a function of the growth rate. *Molecular and General Genetics MGG*, 170(2):225–230, January 1979.

[78] François Lacroute. RNA and protein elongation rates in Saccharomyces cerevisiae. *Molecular and General Genetics MGG*, 125(4):319–327, December 1973.

[79] Joao A. Paulo, Jeremy D. O'Connell, Aleksandr Gaun, and Steven P. Gygi. Proteome-wide quantitative multiplexed profiling of protein expression: Carbon-source dependency in *Saccharomyces cerevisiae*. *Molecular Biology of the Cell*, 26(22):4063–4074, November 2015.

[80] Joao A. Paulo, Jeremy D. O'Connell, Robert A. Everley, Jonathon O'Brien, Micah A. Gygi, and Steven P. Gygi. Quantitative mass spectrometry-based multiplexing compares the abundance of 5000 S. *cerevisiae* proteins across 10 carbon sources. *Journal of Proteomics*, 148:85–93, October 2016.

[81] Andrea Riba, Noemi Di Nanni, Nitish Mittal, Erik Arhné, Alexander Schmidt, and Mihaela Zavolan. Protein synthesis rates and ribosome occupancies reveal determinants of translation elongation rates. *Proceedings of the National Academy of Sciences*, 116(30):15023–15032, July 2019. Publisher: National Academy of Sciences Section: PNAS Plus.

[82] Marlena Siwiak and Piotr Zielenkiewicz. A Comprehensive, Quantitative, and Genome-Wide Model of Translation. *PLOS Computational Biology*, 6(7):e1000865, July 2010. Publisher: Public Library of Science.

[83] C. Waldron and F. Lacroute. Effect of growth rate on the amounts of ribosomal and transfer ribonucleic acids in yeast. *Journal of Bacteriology*, 122(3):855–865, June 1975.

[84] Jianye Xia, Benjamin Sánchez, Yu Chen, Kate Campbell, Sergo Kasvandik, and Jens Nielsen. Proteome allocations change linearly with specific growth rate of *Saccharomyces cerevisiae* under glucose-limitation. Preprint, In Review, May 2021.